

# Anle138b binds predominantly to the central cavity in lipidic A $\beta$ <sub>40</sub> fibrils and modulates fibril formation.

Corresponding Author: Professor Christian Griesinger

**This file contains all reviewer reports in order by version, followed by all author rebuttals in order by version.**

Version 0:

Reviewer comments:

Reviewer #1

(Remarks to the Author)

The work explores the binding of a small molecule drug anle138b to Abeta40 fibrils. The work provides convincing evidence to support their main argument that Anle138b binds inside the central cavity in "pre-treatment" fibrils and binds to the fibrillar surface in fibrils that have been fully formed.

This is a novel and interesting result, the work employs state-of-the-art approaches in ssNMR including ssNMR with signal enhancements by DNP, hence it demonstrates the power of the NMR-based methodology to address this type of question. For these reasons the work would be interesting to a wide audience of researchers.

The manuscript is well written and for the most part is easy to follow. The manuscript is appropriate for publication after adding a bit of clarity on a few minor issues:

- Line 63. "in vitro system developed in prior work". It would be good to add a one-sentence clarification on what this system is.
- In SFig 2c – while the loop region forming the cavity is shown, for greater clarity it would help to add a label pointing to the cavity itself
- Line 102, "liposomes" are mentioned, better specify the lipid type, i.e. "DMPG liposomes"
- SFig 1 shows the aggregation kinetics for various SMPR ratios. In the legend of SFig. 1 it would make sense to show "Anle138b:Ab40" rather than the other way around to match the SMPR parameter
- The "Methods" section needs a bit more detail on how the ssNMR samples were prepared. In many works, fibrils are collected by pelleting using high-speed centrifugation, however, the "Methods" section does not mention that. Specifically, Line 112 mentions the 1D (H)N CP spectra. How was the ssNMR sample prepared so that CP signal strength serves as a measure of fibril formation?
- In line 112-113, negative stain EM is mentioned as a tool supporting fibril formation. Probably, you refer to somewhat higher density fibrils shown in Fig. 1b. of "post-treatment" and "control" samples. From our experience, the fibrillar coverage is not very uniform across the EM-grid, therefore, making a conclusion from a single image is not a very good idea. Please comment on why do you think that negative-stain EM is reliable in your situation.
- In SFig. 2a it makes sense to show the actual data rather than an illustration. SFig 1a does that; it is unclear why SFig 2a should be different.
- Fig. 4a caption says 3D (H)CANH ssNMR spectrum is shown. But the shown spectrum looks more like 2D NCA. You may be showing a projection or a slice within a 3D spectrum, please clarify that.

Reviewer #2

(Remarks to the Author)

Comments on "The clinical drug candidate anle138b binds predominantly to the central cavity in lipidic A $\beta$ <sub>40</sub> fibrils and modulates fibril formation."

This manuscript by Han et al. focuses on understanding the interactions between the small molecular aggregation inhibitor ANLE138b and fibrils of A-beta(1-40). The paper is overall clearly written and the data visualizations are effective. The

overall conclusion is that the small-molecule inhibitor binds predominantly in the fibril core when added before aggregation ("pre-treatment") and predominantly to the fibril surface when added after fibril formation ("post-treatment"). The ssNMR experiments with isotope-labeled amino acids were particularly exciting in terms of developing insights into the specific interactions between drug and target.

However, in parts the data interpretation needs clarification to adequately support their conclusions. The MD simulations do not add that much to the reader's confidence in the findings presented. There are also questions that need clarifying around the experimental design (detailed below). Taken as a whole, the findings are intriguing but a little equivocal, and should be of interest to the A-beta community.

My specific critiques are as follows:

1. For the post-treatment condition, the switch from DMPG to DLPG is not explained. The authors suggest that the DLPG "vesicles" (actually an unknown and ill-defined species) are acting purely as carriers for the drug. ITC data are presented to support a lack of interaction between DLPG and A-beta fibrils – however, ITC would not report on entropically-driven (as opposed to enthalpically-driven) binding. A lack of ITC signal doesn't mean that there is no interaction, especially if predominantly enthalpic interactions (e.g., hydrophobic) are at play. A more established carrier like  $\beta$ -cyclodextrin would have been a better choice.
2. There is a lack of clarity around mass balance. The authors ought to measure how much peptide and how much drug remain in solution at the end of the control, pre-treatment, and post-treatment reactions. How much A-beta assembles into insoluble species, and how much drug co-aggregates with the insoluble states? Without this, it is not possible to understand the stoichiometry of drug:monomer within the fibrils.
3. On a related point, how do the authors explain the observed EM density within the fibril core in the control (0.3) and post-treatment (0.5) conditions? It is implausible that all of the pre-treatment density (0.7) should be assigned to drug if there is a similar contribution in these other conditions.
4. The design of the MD simulations needs more justification. Given that the authors are aiming to simulate lipidic fibrils, they should demonstrate that the conformation of DMPG around the fibrils approximates the ordering experimentally observed by EM. This is especially confusing given how similar the surface interactions of the drug are in the presence vs. absence of DMPG. Furthermore, the simulations with the truncated fibril models seem to be quite biased, with both backbone restraints on flanking residues and positional restraints on the drug molecule, and the drug aligned to the fibril axis. Where else could the drug go than into the central cavity? Finally, it is unclear what exactly the authors define as protonation states for Anle138b? I assume that they mean whether the proton is on the 1- or 2-nitrogen of the pyrazole ring (as opposed to a deprotonated state) but this should be clarified.
5. Figure legends seem to be missing from the main manuscript file.
6. On line 383, the citation should point to ref. 68.

### Reviewer #3

#### (Remarks to the Author)

This is an interesting and well-written manuscript from the Griesinger lab. The authors explore the interaction of Anle138b — with A $\beta$ 40 fibrils under a lipidic environment. Anle138b is a small molecule originally developed in their group and currently undergoing clinical trials for Parkinson's disease and multiple system atrophy. The study employs an impressive suite of biophysical techniques, including cryo-EM, NMR, ITC, molecular dynamics (MD) simulations, and others, to dissect the binding behavior of Anle138b on both pre-formed and forming A $\beta$ 40 fibrils. The key finding is that Anle138b binds within a central hydrophobic cavity of lipid-induced A $\beta$ 40 fibrils (L1 polymorph), interacting with glycine and isoleucine residues, whereas in pre-formed fibrils, it binds more peripherally to solvent-exposed sites without altering the fibril core. These insights are valuable for guiding future rational design of amyloid-targeting therapeutics. I have a few suggestions to improve the manuscript:

- (1) Throughout the manuscript, the term "lipidic A $\beta$ " is used, which may be misleading. In some contexts, this term could imply covalent linkage between lipids and A $\beta$ . However, in this work, the authors refer to fibrils formed in the presence of lipids (specifically DMPG), not covalently modified A $\beta$ . The authors should clarify this to avoid potential confusion.
- (2) DMPG is used for co-incubation during fibril formation (pre-treatment), while DLPG is used to deliver Anle138b in post-treatment conditions. The rationale behind this choice should be explicitly addressed in the manuscript. Given that DMPG and DLPG differ in fluidity and fatty acid chain length, these lipids may influence the compound's interaction with A $\beta$  differently. Furthermore, it is not clear whether the pre-formed fibrils used in the post-treatment experiments were also generated in the presence of lipids or in their absence. Clarifying this will help contextualize the differences observed.
- (3) The manuscript lacks information on the molar ratios of lipid to A $\beta$  and lipid to Anle138b. These parameters are crucial, as varying lipid concentrations can significantly affect A $\beta$  aggregation pathways and compound accessibility.

(4)The authors report a significant reduction in  $\beta$ -sheet content after 48 hours of incubation with Anle138b, based on CD spectra (Fig. S1C). However, the presented spectra only show modest shifts in the characteristic  $\beta$ -sheet peaks, as the positive peak slightly increases and negative peak value is a bit higher. To strengthen the conclusion, the authors should consider performing secondary structure deconvolution of the CD data to quantify the percentage of  $\beta$ -sheet content.

(5)NMR results (Fig. 1C) show a marked reduction in fibrillar signal upon Anle138b treatment in the pre-treatment condition, suggesting reduced fibril formation. In contrast, ssNMR in Fig.3 indicates that the compound can bind within the fibril core. These findings seem partially contradictory. Does Anle138b destabilize early fibril formation but remain stably bound in the formed fibril? Could the central binding pocket identified in figure 3 also play a role in modulating primary nucleation? Further discussion on how the structural data correlate with the dissolution or prevention of fibril formation would be valuable.

(6)To reinforce the functional relevance of the identified binding site, the authors might consider performing mutagenesis on key residues within the cavity (e.g., glycine or isoleucine residues) and assessing the effect on compound binding and fibril dissolution. This would provide mechanistic support for the role of the binding pocket in compound action against fibril formation.

(7)The conclusion that Anle138b competes with ThT for binding may be premature. ThT fluorescence can be influenced by multiple factors, including fibril structure and accessibility. To confirm direct competition, the authors could fix the compound concentration and titrate increasing amounts of ThT to observe potential displacement effects. Such data would help validate this claim.

(8)In the ITC experiments, the compound is solubilized in DLPG. It is unclear, however, whether the A $\beta$  fibrils used in these experiments (post-treatment) were also prepared in DLPG or in a different lipid or buffer system. Since pre- and post-treatment experiments involve different lipids (DMPG vs. DLPG), this could affect the comparability of binding data and should be clarified.

(9)The authors apply a flat-bottomed positional restraint in their MD simulations. More explanation is needed regarding the purpose of this restraint and whether it might limit the natural flexibility of the compound-fibril interaction. Could this influence the binding mode or energetics observed?

#### Reviewer #4

##### (Remarks to the Author)

I co-reviewed this manuscript with one of the reviewers who provided the listed reports. This is part of the Nature Communications initiative to facilitate training in peer review and to provide appropriate recognition for Early Career Researchers who co-review manuscripts.

#### Version 1:

##### Reviewer comments:

#### Reviewer #1

##### (Remarks to the Author)

The authors have addressed all the minor issues that I've raised in the first review round. The manuscript should be good for publication.

#### Reviewer #2

##### (Remarks to the Author)

I appreciate the authors' responsiveness and clarity. However, their revisions leave a couple of issues that I believe still need to be addressed:

1. I was confused by the rationale that that DLPG was selected to reduce charge-based nonspecific interactions, given that DLPG and DMPG have the same head group and charge state. The subsequent parallel rationale based on membrane phase and fluidity, while speculative, is clearer and more plausible.

2. The initial version of the manuscript clearly explained that the DLPG is likely to be in a micelle-like state and is referred to as 'vesicles' only for convenience. This is an essential disclosure that has been lost in the revision, and I believe it needs to be added back to the manuscript.

Other than those caveats, in my opinion this is a really nicely executed and presented piece of work.

#### Reviewer #3

(Remarks to the Author)

The authors have satisfactorily addressed my concerns, and I recommend acceptance of the manuscript in its current form.

Reviewer #4

(Remarks to the Author)

I co-reviewed this manuscript with one of the reviewers who provided the listed reports. This is part of the Nature Communications initiative to facilitate training in peer review and to provide appropriate recognition for Early Career Researchers who co-review manuscripts.

**Open Access** This Peer Review File is licensed under a Creative Commons Attribution 4.0 International License, which permits use, sharing, adaptation, distribution and reproduction in any medium or format, as long as you give appropriate credit to the original author(s) and the source, provide a link to the Creative Commons license, and indicate if changes were made.

In cases where reviewers are anonymous, credit should be given to 'Anonymous Referee' and the source.

The images or other third party material in this Peer Review File are included in the article's Creative Commons license, unless indicated otherwise in a credit line to the material. If material is not included in the article's Creative Commons license and your intended use is not permitted by statutory regulation or exceeds the permitted use, you will need to obtain permission directly from the copyright holder.

To view a copy of this license, visit <https://creativecommons.org/licenses/by/4.0/>

## REVIEWER COMMENTS

Reviewer #1 (Remarks to the Author):

The work explores the binding of a small molecule drug anle138b to Abeta40 fibrils. The work provides convincing evidence to support their main argument that Anle138b binds inside the central cavity in “pre-treatment” fibrils and binds to the fibrillar surface in fibrils that have been fully formed. This is a novel and interesting result, the work employs state-of-the-art approaches in ssNMR including ssNMR with signal enhancements by DNP, hence it demonstrates the power of the NMR-based methodology to address this type of question. For these reasons the work would be interesting to a wide audience of researchers. The manuscript is well written and for the most part is easy to follow. The manuscript is appropriate for publication after adding a bit of clarity on a few minor issues:

**- Line 63. “in vitro system developed in prior work”. It would be good to add a one-sentence clarification on what this system is.**

Good point. We have revised the manuscript to provide a clearer description of the in vitro system in response to your comment. The revisions are reflected in lines 63- 64 (highlighted in red) of the manuscript, as shown below.

*Lines 62-66:* Among these polymorphs, the type 1 lipidic A $\beta$ <sub>40</sub> fibril<sup>18-20</sup> is predominantly observed when the protein is allowed to aggregate in the presence of negatively charged DMPG lipid vesicles (lipid-to-protein molar ratio (LPR) = 30:1) at pH 6.5 and 37°C, as reported previously<sup>18</sup>. This fibril type, henceforth referred to as the L1 A $\beta$ <sub>40</sub> fibril, has been shown to resemble the pathological structures observed in the brains of patients.

**- In SFig 2c – while the loop region forming the cavity is shown, for greater clarity it would help to add a label pointing to the cavity itself**

We followed the suggestion and have added a label and arrow in the revised figure as recommended.

**- Line 102, “liposomes” are mentioned, better specify the lipid type, i.e “DMPG liposomes”**

We have changed it to “DMPG liposomes” and changed “liposomes” in line 108 to “DMPG liposome” for consistency highlighted.

**- SFig 1 shows the aggregation kinetics for various SMPR ratios. In the legend of SFig. 1 it would make sense to show “Anle138b: Ab40” rather than the other way around to match the SMPR parameter**

In line with your comment, we have revised the molar ratio notation in the SFig. 1 legend to match the SMPR definition (anle138b: A $\beta$ <sub>40</sub> molar ratio). We have also applied the same notation consistently in the legends of Main Figures 1, 3, 4, 5, and Supplementary Figures 1, 3, 4, 5, 11, 12, 13, and 16. All revisions are reflected in the new manuscript with changes highlighted in red.

**- The “Methods” sections needs a bit more detail on how the ssNMR samples were prepared. In many works, fibrils are collected by pelleting using high-speed centrifugation, however, the “Methods” section does not mention that. Specifically, Line 112 mentions the 1D (H)N CP spectra. How was the ssNMR sample prepared so that CP signal strength serves as a measure of fibril formation?**

We have revised the 'Methods' section to clarify this point. Specifically, we have added the information that both pre-treatment and post-treatment fibrils were collected by high-speed centrifugation prior to ssNMR measurements. This information has been added in red at lines 469-472 (**highlighted in red**) of the revised manuscript, as shown below.

**Lines 466- 472:** The anle138b-loaded DLPG vesicles were used to treat preformed L1 A $\beta$ <sub>40</sub> fibrils for subsequent ITC, DNP-NHHC, HCANH titration, **ssNMR**, and Cryo-EM experiments. With the exception of the ITC experiment, L1 A $\beta$ <sub>40</sub> fibrils were incubated at 37 °C for 1 hour to allow sufficient interaction prior to measurement. **The fibrils were collected by high-speed centrifugation at 55,000 g for 60 minutes for subsequent ssNMR measurements. The pelleted fibrils were then packed into MAS rotors using a funnel consisting of a trimmed pipette tip and a tabletop centrifuge.**

**- In line 112-113, negative stain EM is mentioned as a tool supporting fibril formation. Probably, you refer to somewhat higher density fibrils shown in Fig. 1b. of “post-treatment” and “control” samples. From our experience, the fibrillar coverage is not very uniform across the EM-grid, therefore, making a conclusion from a single image is not a very good idea. Please comment on why do you think that negative-stain EM is reliable in your situation.**

We agree that negative-stain EM images should not be used as an independent quantitative tool. In this manuscript, they formed part of a cross-validation process alongside NMR, ThT fluorescence analysis, and CD

spectra, all of which were obtained from the same sample. This is specified in the legends of Supplementary Figures 3 (panels a and b) and 5, thereby strengthening the reliability of our conclusions regarding fibril formation and quantity.

**- In SFig. 2a it makes sense to show the actual data rather than an illustration. SFig 1a does that; it is unclear why SFig 2a should be different.**

We chose to present Supplementary Figure 2a as a schematic to provide a clear summary of the aggregation kinetics before and after anle138b administration. The corresponding experimental data are shown in Supplementary Figure S1a (for pre-aggregation) and Figure 1c (for both pre- and post-aggregation). Unlike Supplementary Figure 1a, which presents raw kinetic traces, Supplementary Figure 2a is intended to give readers a conceptual overview of the experimental timeline and treatment point. We have revised the figure legend accordingly to clarify this purpose. This has been highlighted in red for your reference.

**Supplementary Figure 2 | Schematic illustration of experiments investigating the binding sites of anle138b on L1 A $\beta$ <sub>40</sub> fibrils.**

a. Schematic illustration of L1 A $\beta$ <sub>40</sub> fibril formation under pre-treatment and post-treatment conditions. In the post-treatment condition, anle138b (blue) is added after fibril formation. In the pre-treatment condition, fibrils form in the presence of anle138b (red), which extends the lag phase and reduces the final fibril amount. The two arrows indicate the time points at which anle138b was administered during the fibril formation process. Blue represents the post-treatment condition, and red represents the pre-treatment condition. This schematic provides a conceptual overview of the experimental timeline and administration of anle138b, complementing the corresponding kinetic data shown in Supplementary Fig. 1a and Fig. 1c.

**- Fig. 4a caption says 3D (H)CANH ssNMR spectrum is shown. But the shown spectrum is looks more like 2D NCA. You may be showing a projection or a slice within a 3D spectrum. Please clarify that.**

Thank you for your comment. The spectrum shown in Fig. 4a is indeed a 2D projection of the 3D (H)CANH ssNMR spectrum. We have clarified this in the figure legend to avoid confusion, and the corresponding revision has been highlighted in red in the updated manuscript.

**Fig. 4: Titration of anle138b binding to L1 A $\beta$ <sub>40</sub> fibrils under post-treatment conditions.**

a. 3D (H)CANH solid-state NMR spectra of L1 A $\beta$ <sub>40</sub> fibrils titrated with increasing concentrations of anle138b (anle138b: A $\beta$ <sub>40</sub> molar ratio (SMPR) from 0 to 1.2). The spectrum shown is a 2D projection of the 3D spectrum. Chemical shift perturbations (CSPs) and signal intensity reductions are observed upon treatment with anle138b. Residues exhibiting both CSPs and signal attenuation are marked in pink arrows; those showing CSPs only are marked in gray arrows. Peaks for residues K16, D23, S26, and K28 (highlighted in purple) become undetectable at the highest anle138b concentration.

## Reviewer #2 (Remarks to the Author):

Comments on “The clinical drug candidate anle138b binds predominantly to the central cavity in lipidic A $\beta$ <sub>40</sub> fibrils and modulates fibril formation.”

This manuscript by Han et al. focuses on understanding the interactions between the small molecular aggregation inhibitor ANLE138b and fibrils of A-beta(1-40). The paper is overall clearly written and the data visualizations are effective. The overall conclusion is that the small-molecule inhibitor binds predominantly in the fibril core when added before aggregation (“pre-treatment”) and predominantly to the fibril surface when added after fibril formation (“post-treatment”). The ssNMR experiments with isotope-labeled amino acids were particularly exciting in terms of developing insights into the specific interactions between drug and target. However, in parts the data interpretation needs clarification to adequately support their conclusions. The MD simulations do not add that much to the reader’s confidence in the findings presented. There are also questions that need clarifying around the experimental design (detailed below). Taken as a whole, the findings are intriguing but a little equivocal, and should be of interest to the A-beta community.

Thank you for the overall positive assessment. We are well aware, as pointed out, that the MD simulations have particular limitations, for example, in the timescale that is feasible to simulate. Still, they add value to the manuscript, since the snapshots from the MD confirm the physical ‘reasonableness’ of the proposed binding interactions, and also help to clarify possible binding poses.

My specific critiques are as follows:

**1. For the post-treatment condition, the switch from DMPG to DLPG is not explained. The authors suggest that the DLPG “vesicles” (actually an unknown and ill-defined species) are acting purely as carriers for the drug. ITC data are presented to support a lack of interaction between DLPG and A-beta fibrils – however, ITC would not report on entropically-driven (as opposed to enthalpically-driven) binding. A lack of ITC signal doesn’t mean that there is no interaction, especially if predominantly enthalpic**



**interactions (e.g., hydrophobic) are at play. A more established carrier like  $\beta$ -cyclodextrin would have been a better choice.**

We appreciate the reviewer's valuable comment. In the post-treatment condition, DLPG was used to deliver anle138b directly to pre-formed L1 A $\beta$ <sub>40</sub> fibrils. These fibrils are structurally identical to those used in the pre-treatment and control conditions, as all were formed under the same DMPG-containing conditions. In these cases, DMPG was used as a lipid that promotes fibril formation, and both cryo-EM density maps and ssNMR NOE analyses confirmed that DMPG is bound to the fibril surface<sup>18</sup>. The structural characteristics of DMPG binding are described in greater detail in response to Reviewer #3's Comment 1 and have been addressed in the revised manuscript (Lines 75–77, [highlighted in blue](#)).

DMPG carries a negative charge and engages in hydrophobic interactions with the fibril surface. To avoid such charge-based interactions involving the DMPG head group, DLPG was selected as an alternative. DLPG also carries a negative charge but has a lower melting temperature ( $T_m = -3\text{ }^{\circ}\text{C}$ ), which results in high membrane fluidity at the experimental temperature ( $25\text{ }^{\circ}\text{C}$ ). This property facilitates the dispersion and release of hydrophobic molecules such as anle138b. Therefore, DLPG provides a favorable environment for solubilizing and delivering the drug while minimizing nonspecific binding to A $\beta$ <sub>40</sub> fibrils. This has been reflected in the revised manuscript (Lines 453–459, [highlighted in green](#)).

**Lines 453–459:** For post-treatment conditions, DLPG vesicles were used to deliver anle138b to pre-formed L1 A $\beta$ <sub>40</sub> fibrils. DLPG was selected instead of DMPG to reduce potential charge-based nonspecific interactions, as DLPG headgroups are less prone to stable association with the fibril surface. Additionally, DLPG has a lower melting temperature ( $T_m = -3\text{ }^{\circ}\text{C}$ ), which ensures high membrane fluidity at  $25\text{ }^{\circ}\text{C}$  and facilitates dispersion of hydrophobic molecules such as anle138b. To minimize co-sedimentation artifacts during centrifugation, small unilamellar DLPG vesicles were used.

No detectable interaction between DLPG and L1 A $\beta$ <sub>40</sub> fibrils was observed using three independent methods: ITC, ssNMR NOE, and cryo-EM. Acknowledging that ITC alone may not capture all types of interactions, we employed additional analyses using ssNMR NOE and cryo-EM to assess the potential binding between DLPG and A $\beta$ <sub>40</sub> fibrils comprehensively. All three techniques consistently failed to detect any interaction signals, thereby compensating for the limitations of any single method. *Together, these findings confirm that DLPG served as a non-interacting delivery vehicle in our system.* This has been included in the revised manuscript (Lines 230–233, [highlighted in green](#)).

**Lines 230–233:** DLPG vesicles lacking anle138b produced no measurable heat signal in ITC (Supplementary Fig. 13b, Supplementary Table 2). This absence of detectable interaction was corroborated by ssNMR NOE and cryo-EM, which showed no DLPG-specific contacts or densities on the L1 A $\beta$ <sub>40</sub> fibril surface (Fig. 2b, Fig. 5).

We appreciate the reviewer's suggestion to use  $\beta$ -cyclodextrin as a potential delivery vehicle. Unfortunately, we have not been able to solubilize Anle138b in  $\alpha$ -,  $\beta$ -, or  $\gamma$ -cyclodextrin. Furthermore, previous studies have shown that  $\beta$ -cyclodextrin can itself influence A $\beta$  aggregation by inhibiting fibril formation or

disassembling pre-formed fibrils<sup>1</sup> (Shinde et al., 2017). Moreover,  $\beta$ -cyclodextrin has been reported to form inclusion complexes with amyloid peptides themselves<sup>2,3</sup> (Yang et al., 2012; Qin et al., 2002), which could further complicate the interpretation of anle138b's independent effects on fibril formation. Since the objective of this study was to isolate the effects of anle138b alone,  $\beta$ -cyclodextrin was intentionally excluded.

1. Shinde, Meenakshi N., et al. "Sulfobutylether- $\beta$ -cyclodextrin for inhibition and rupture of amyloid fibrils." *The Journal of Physical Chemistry C* 121.36 (2017): 20057-20065.
2. Wahlstrom, Anna, et al. "Specific binding of a  $\beta$ -cyclodextrin dimer to the amyloid  $\beta$  peptide modulates the peptide aggregation process." *Biochemistry* 51.21 (2012): 4280-4289.
3. Qin, Xu-rong, Hiroshi Abe, and Hiroshi Nakanishi. "NMR and CD studies on the interaction of Alzheimer  $\beta$ -amyloid peptide (12–28) with  $\beta$ -cyclodextrin." *Biochemical and biophysical research communications* 297.4 (2002): 1011-1015.

**2. There is a lack of clarity around mass balance. The authors ought to measure how much peptide and how much drug remain in solution at the end of the control, pre-treatment, and post-treatment reactions. How much A-beta assembles into insoluble species, and how much drug co-aggregates with the insoluble states? Without this, it is not possible to understand the stoichiometry of drug:monomer within the fibrils.**

We appreciate the reviewer's valuable comment.

Using CD spectroscopy and solution-state NMR, we confirmed that under both control and post-treatment (pre-formed fibril) conditions, A $\beta$ <sub>40</sub> monomers were completely converted into insoluble fibrils. In the pre-treatment condition, the CD spectra showed the disappearance of random coil signals and the emergence of  $\beta$ -strand signatures. Additionally, ssNMR INEPT HN-H spectra did not show signals corresponding to free monomers or unstructured peptide states. The data collectively support that A $\beta$ <sub>40</sub> is predominantly found in the fibrillar form under both control and post-treatment conditions. Supplementary Figure 3 panels c and d include additional ThT fluorescence and CD spectrum data from the supernatant after fibril formation.

Regarding drug binding, ITC analysis showed no significant heat change between DLPG vesicles and A $\beta$ <sub>40</sub> fibrils, whereas a clear exothermic signal was observed between anle138b-loaded DLPG vesicles and A $\beta$ <sub>40</sub> fibrils. This supports that anle138b directly interacts with the fibrils. Furthermore, ssNMR titration experiments performed under the same conditions revealed a similar stoichiometry, further supporting the interaction between the drug and fibrils.

Moreover, 1D solution-state <sup>1</sup>H NMR analysis of the supernatant from post-treatment samples (after ultracentrifugation) revealed no detectable anle138b signals at SMPR ratios of 0.2:1 and 0.8:1, whereas ~30% of free drug remained at a ratio of 1.2:1. These results suggest that, under these conditions, the majority of anle138b is incorporated into fibrils. The corresponding 1D <sup>1</sup>H NMR spectra are shown in Supplementary Figures 21 and

22 and have been reflected in the revised manuscript (Lines 127–133, Lines 220–233, Lines 375–377; highlighted in green).

**Lines 127–134** This observation was supported by analysis of the supernatant following ultracentrifugation: CD and ThT fluorescence spectra showed that  $\beta$ -strand-like species remained in the supernatant under pre-treatment conditions, indicating the presence of soluble, non-fibrillar  $A\beta_{40}$  aggregates (Supplementary Fig. 3c, d). In contrast, these species were absent in the control or post-treatment samples, where nearly all  $A\beta_{40}$  sedimented as fibrils (Supplementary Fig. 3c, d), i.e. post-treatment resulted in no significant change in fibril quantity (Fig. 1c, Supplementary Fig. 3b).

**Lines 220–233:** CD spectroscopy and ThT fluorescence confirmed full conversion of  $A\beta_{40}$  monomers into fibrils under both control and post-treatment conditions, consistent with near-complete sedimentation of L1  $A\beta_{40}$  after ultracentrifugation (Supplementary Fig. 3).

To further assess drug incorporation, we analyzed the supernatant after ultracentrifugation using 1D solution NMR. No free anle138b signal was detected at anle138b:  $A\beta_{40}$  ratios of 0.2:1 and 0.8:1, while ~30% of the drug remained unbound at a 1.2:1 ratio (Supplementary Figs. 21, 22). These results align with the stoichiometry measured by ITC (Fig. 4b, Supplementary Table 2) and NMR titration (Fig. 4a). Together, they indicate that the majority of anle138b associates with the fibrils.

DLPG vesicles lacking anle138b produced no measurable heat signal in ITC (Supplementary Fig. 13b, Supplementary Table 2). This absence of detectable interaction was corroborated by ssNMR NOE and cryo-EM, which showed no DLPG-specific contacts or densities on the L1  $A\beta_{40}$  fibril surface (Fig. 2b, Fig. 5).

**Lines 375–377:** These results are further supported by ultracentrifugation analysis of the supernatant under post-treatment conditions, confirming near complete conversion of  $A\beta_{40}$  into fibrils and a substantial incorporation of anle138b into the fibril fraction.

Given the lipidic nature of the fibrils used in this study, it is technically challenging to distinguish whether the drug is bound to the fibril core or to the surrounding lipid assemblies using conventional mass-based quantification methods. Therefore, the quantification of drug–fibril interactions was based on ITC and ssNMR, which represent the most reliable and informative approaches available for this system. We acknowledge that further development of complementary techniques will be necessary to determine the absolute amount and site-specificity of drug binding with greater resolution in future studies.

Accordingly, we focused on ITC and NMR titration experiments to provide the most quantitative and reliable evaluation of drug–fibril interactions and their stoichiometry within the scope of this study.

**3. On a related point, how do the authors explain the observed EM density within the fibril core in the control (0.3) and post-treatment (0.5) conditions? It is implausible that all of the pre-treatment density (0.7) should be assigned to drug if there is a similar contribution in these other conditions.**

We indeed don't know what the density is in the control fibrils and therefore refrained from a detailed discussion on potential water or side chains occupying this space. Clearly, in the control but also in the post-treatment condition, the contribution from anle138b is not sufficient to induce peaks in the DNP-NHHC experiments. Those peaks, which directly confirm that anle138b binds within the fibril core, were only observed under the pre-treatment condition. Based on these results, we interpret the increased core density in the pre-treatment sample as reflecting more anle138b binding in the cavity than in the post-treatment sample. While we do not attribute the entire 0.7 density solely to the drug, the relative increase, compared to control and post-treatment, supports the presence of anle138b in the core.

**4. The design of the MD simulations needs more justification. Given that the authors are aiming to simulate lipidic fibrils, they should demonstrate that the conformation of DMPG around the fibrils approximates the ordering experimentally observed by EM. This is especially confusing given how similar the surface interactions of the drug are in the presence vs. absence of DMPG. Furthermore, the simulations with the truncated fibril models seem to be quite biased, with both backbone restraints on flanking residues and positional restraints on the drug molecule, and the drug aligned to the fibril axis. Where else could the drug go than into the central cavity? Finally, it is unclear what exactly the authors define as protonation states for Anle138b? I assume that they mean whether the proton is on the 1- or 2-nitrogen of the pyrazole ring (as opposed to a deprotonated state) but this should be clarified.**

We thank the reviewer for this suggestion. The MD simulation methods section has been revised accordingly to include the relevant details (highlighted in green).

● DMPG Conformation and Comparison to cryo-EM and ssNMR Data

We've enhanced our analysis of the MD simulations by incorporating average density grids and interaction frequencies to more thoroughly characterize the DMPG conformation around the L1 fibrils (Supplementary Figure 23, see MD simulation methods section for details). We acknowledge that the simulations, performed at 300 K, may not fully replicate the lipid ordering seen in cryo-EM. However, the lipid-binding regions

and lipid-fibril interactions, as found in the cryo-EM and ssNMR experiments depicted in Figures 2 and 5, are well-approximated. Furthermore, the interatomic contacts of surface-bound anle138b (Supplementary Fig. 18) reveal significant differences in the distributions of minimum distances between anle138b pyrazole nitrogen atoms and all N or C atoms of residues I31 and I32, both with and without DMPG. Notably, we observed no close I32–anle138 b contacts in the presence of lipids, suggesting competition of lipid and anle138b binding at the L1 A $\beta$ <sub>40</sub> fibril surface near the position of Ile32. This has been included in the revised manuscript (Lines 294–295, highlighted in green).

**Lines 291–296:** Notably, anle138b did not bind to the central cavity in either lipid-containing or lipid-free simulations. Lipid-free simulations show short distances (below 5 Å) between the pyrazole NH of anle138b and C $\delta$  of residue Ile32, consistent with NMR data, while the lipid-containing simulations do not, suggesting competition of lipid and anle138b binding at the L1 A $\beta$ <sub>40</sub> fibril surface near the position of Ile32 (Fig. 6b, c, Supplementary Fig.18a, b).

#### ● Use of Restraints and Sampling of Central Cavity Binding

The central, ringlike cavity located along the fibril axis is narrow with a maximal diameter of approximately 1 nm. We carried out MD simulations on a truncated fibril model specifically designed to answer the questions a) is anle138b (sterically) able to bind to the central cavity, b) dynamic inside the fibril binding site, and c) reproducing the interatomic protein-ligand contacts observed in the NMR experiments. To remove the possible bias from initial configurations, we opted to start from ligand positions outside of the fibril with no fibril-ligand contacts, instead of, e.g., a docked pose inside the central cavity. No biasing forces were applied to steer the ligand into the central cavity. To keep the diffusion of the small molecule in the simulation box restricted to a cylindrical volume centered on the binding site of interest, the radius of the flat-bottom potential was chosen to correspond with the geometry of the ring-like cavity and the full extension of anle138b. This approach reduces computational cost significantly and increases the sampling efficiency of binding events to the cavity of the L1 A $\beta$ <sub>40</sub> fibril polymorph by preventing the compound from binding in a different site on the fibril surface. The flat-bottom potential, however, does not impede the compound to freely rotate, orient, un- and rebind from the fibril (cavity); it results in no forces when the molecule is bound, or just outside the entrance of the cavity. The orientational alignment of unbound anle138b is shown in Supplementary Figure 24.

During the production MD simulations of the truncated fibrils, the initial atomic coordinates of the C $\alpha$  atoms of protein residues Gln15-Lys16 and Val36-Val40 were restrained using a harmonic potential with a force constant of 1000 kJ mol<sup>-1</sup> nm<sup>-2</sup> to ensure that the fibril models were stable, preserving the initial fold of the N- and C-terminal regions of the L1 A $\beta$ <sub>40</sub> fibril as resolved by cryo-EM. The restrained atoms mainly serve to avoid undesired shearing and twisting of the protofilaments and are more than 1.5 nm away from the residues located near and around the central cavity, while the rest of all protein atoms are free from restraining forces. While the chosen design does restrict the conformational space of the ligand such that the simulations will only capture a subset of the possible binding sites, i.e. the central cavity and the tip of the fibril, the simulations do not bias towards or reinforce a specific pose. See also reply to comments (9) of [Reviewer #3 on p. 16](#). We revised the Method Section to improve the clarity regarding the setup and implications of the use of flat-bottomed potentials in the simulations with truncated fibril models.

- Protonation states for Anle138b

Indeed, both proton positions (1-nitrogen and 2-nitrogen) were simulated. The nomenclature in the Method Section has been adjusted such that the description is not confused with protonated vs deprotonated states of the pyrazole ring. (Lines 624-625, Lines 652–654; highlighted in green).

**Lines 623–625:** Based on this principal simulation system, two setups were built by adding the small molecule anle138b (representing both possible proton positions on the pyrazole ring; 1-nitrogen and 2-nitrogen in a 1:1 ratio):

**Lines 650–654:** For the initial configuration, one anle138b molecule was placed outside and above the central cavity of the loop region of L1 A $\beta$ <sub>40</sub> fibril, such that the long axis of the small molecule aligned with the fibril axis. For this simulation system, five independent NPT production simulations were carried out per possible proton position on the pyrazole nitrogens of anle138b, each 5.0  $\mu$ s long.

## 5. Figure legends seem to be missing from the main manuscript file.

We thank the reviewer for the comment. In the revised manuscript, all figure legends have been clearly included in the main file. We will make sure to check such details more carefully in future submissions.

## 6. On line 383, the citation should point to ref. 68.

Thank you for your comment. We have corrected the citation to refer to Ref. 68 (Green color), and this change has been implemented on line 386 of the revised manuscript.

### Reviewer #3 (Remarks to the Author):

This is an interesting and well-written manuscript from the Griesinger lab. The authors explore the interaction of Anle138b —with A $\beta$ 40 fibrils under a lipidic environment. Anle138b is a small molecule originally developed in their group and currently undergoing clinical trials for Parkinson's disease and multiple system atrophy. The study employs an impressive suite of biophysical techniques, including cryo-EM, NMR, ITC, molecular dynamics (MD) simulations, and others, to dissect the binding behavior of Anle138b on both pre-formed and forming A $\beta$ 40 fibrils. The key finding is that Anle138b binds within a central hydrophobic cavity of lipid-induced A $\beta$ 40 fibrils (L1 polymorph), interacting with glycine and isoleucine residues, whereas in pre-formed fibrils, it binds more peripherally to solvent-exposed sites without altering the fibril core. These insights are valuable for guiding future rational design of amyloid-targeting therapeutics. I have a few suggestions to improve the manuscript:

**(1) Throughout the manuscript, the term “lipidic A $\beta$ ” is used, which may be misleading. In some contexts, this term could imply covalent linkage between lipids and A $\beta$ . However, in this work, the authors refer to fibrils formed in the presence of lipids (specifically DMPG), not covalently modified A $\beta$ . The authors should clarify this to avoid potential confusion.**

We thank the reviewer for the valuable comments. To avoid any misunderstanding that the term “lipidic A $\beta$ ” implies covalent linkage between lipids and A $\beta$ , we have revised the manuscript to clarify that the fibrils were formed in the presence of DMPG, with **non-covalent** lipid interactions. The revisions are reflected in *lines 75–77 (highlighted in blue)* of the manuscript, as shown below.

*Lines 74-77:* This cavity is centrally located along the fibril axis and is hereafter referred to as the central cavity (Supplementary Fig. 2b, c). The L1 A $\beta$ <sub>40</sub> fibril is formed in the presence of DMPG liposomes, where lipid acyl chains interact with hydrophobic surfaces of the fibril (L17–F19 and A30–V36) through non-covalent interactions<sup>18</sup>.

**(2) DMPG is used for co-incubation during fibril formation (pre-treatment), while DLPG is used to deliver Anle138b in post-treatment conditions. The rationale behind this choice should be explicitly addressed in the manuscript. Given that DMPG and DLPG differ in fluidity and fatty acid chain length, these lipids may influence the compound's interaction with A $\beta$  differently. Furthermore, it is not clear whether the pre-formed fibrils used in the post-treatment experiments**

were also generated in the presence of lipids or in their absence. Clarifying this will help contextualize the differences observed.

We thank the reviewer for the comment. This comment regarding DLPG and DMPG overlaps with the first comment from Reviewer #2, and the related explanation and experimental data were provided in that response.

Hydrophobic compounds such as anle138b generally have low aqueous solubility. Forming complexes with cyclodextrin or serum albumin is one of the strategies used to increase the solubility of such compounds. In this study, DLPG was used for solubilization and delivery of anle138b.

The system is based on fibrils formed in the presence of DMPG, which interacts with the L1 A $\beta$ <sub>40</sub> fibril surface through hydrophobic interactions. In the post-treatment condition, DLPG was used to deliver anle138b. DLPG has high membrane fluidity at room temperature and shows less nonspecific interaction via charge-based effects with L1 A $\beta$ <sub>40</sub> fibrils formed in the presence of DMPG.

Under the experimental conditions, DMPG tended to form relatively large vesicles compared to DLPG. These larger vesicles could affect sample recovery through ultracentrifugation in ssNMR experiments, and therefore, DLPG was used in the post-treatment condition. To match the conditions used in ssNMR titration, DLPG was also used in the ITC experiment.

The fibril formation conditions used in the post-treatment experiments are described in lines 125–126 of the manuscript (highlighted in blue).

**Lines 121-126:** To evaluate the effect of anle138b at different stages of fibril formation, we compared three experimental conditions: 1) pre-treatment (SMPR = 1.2, with anle138b added before initiating fibril formation), 2) post-treatment (SMPR = 1.2, with anle138b applied after fibril formation was completed), and 3) control (fibril without anle138b) (Supplementary Fig. 2a). Pre-formed fibrils used in the post-treatment condition were generated with DMPG liposomes under identical conditions to the control fibrils.

**(3) The manuscript lacks information on the molar ratios of lipid to A $\beta$  and lipid to Anle138b. These parameters are crucial, as varying lipid concentrations can significantly affect A $\beta$  aggregation pathways and compound accessibility.**

We thank the reviewer for this helpful comment. We have revised the manuscript to include the molar ratio of lipid to A $\beta$ <sub>40</sub> (LPR = 30:1) in the description of the in vitro system, as reflected in lines 63–64 (highlighted in red), and previously noted in our response to Reviewer #1 (1<sup>st</sup> comment). Regarding the molar ratio of lipid to Anle138b, we have added this information to the Methods section. Specifically, the A $\beta$ <sub>40</sub>: DMPG: anle138b molar ratios have been included in the “*L1 A $\beta$ <sub>40</sub> fibril preparation*” and “*Aggregation assay*” subsections to clarify experimental conditions. The main text and figure legends refer to SMPR values to maintain consistency in data interpretation, while the full molar ratios are now provided in the Methods section for reference. These revisions



are reflected in lines 63-64(highlighted in red), 442-444, and 476 (highlighted in blue) of the manuscript, as shown below.

**Lines 62-66:** Among these polymorphs, the type 1 lipidic A $\beta_{40}$  fibril<sup>18-20</sup> is predominantly observed when the protein is allowed to aggregate in the presence of negatively charged DMPG lipid vesicles (lipid-to-protein molar ratio (LPR) = 30:1) at pH 6.5 and 37°C, as reported previously<sup>18</sup>. This fibril type, henceforth referred to as the L1 A $\beta_{40}$  fibril, has been shown to resemble the pathological structures observed in the brains of patients.

**Lines 440-445:** For fibril formation experiments, the DMPG film was hydrated and sonicated in 10 mM sodium phosphate buffer (pH 6.5) for 5 minutes to generate vesicles that promote A $\beta_{40}$  aggregation. Under the pre-treatment fibril condition, anle138b was incorporated into DMPG during lipid film preparation to produce vesicles containing both lipid and anle138b (LPR = 30:1, SMPR = 0.2-1.2). Control fibrils and pre-treatment fibrils were formed with DMPG liposomes with or without anle138b.

**Lines 474-476:** Aggregation assays were conducted under the same lipidic conditions used for fibril formation, either with DMPG liposomes (SUV) alone (control fibril condition) or with DMPG liposomes (SUV) containing anle138b (LPR = 30:1, SMPR = 0.6 or 1.2).

**(4) The authors report a significant reduction in  $\beta$ -sheet content after 48 hours of incubation with Anle138b, based on CD spectra (Fig. S1C). However, the presented spectra only show modest shifts in the characteristic  $\beta$ -sheet peaks, as the positive peak slightly increases and negative peak value is a bit higher. To strengthen the conclusion, the authors should consider performing secondary structure deconvolution of the CD data to quantify the percentage of  $\beta$ -sheet content.**

We appreciate the reviewer's thoughtful feedback.

Supplementary Fig. 1C presents kinetic data monitored in real-time using ThT fluorescence with a Tecan plate reader. After 48 hours of monitoring ThT-containing samples with the plate reader, the same samples were immediately analyzed by CD spectroscopy, and the corresponding results are shown in Supplementary Fig. 1C.

To further clarify  $\beta$ -sheet formation and secondary structural characteristics, we performed additional analyses on the same samples prepared at the highest concentration of Anle138b (SMPR=1.2). These analyses involved various methods including CD spectroscopy, ThT fluorescence, ssNMR, and cryo-EM, and the comprehensive structural evaluations are presented in Fig. 1, 2, and Supplementary Fig. 3 and 5.

The CD spectra shown in Supplementary Fig. 3 exhibit typical  $\beta$ -sheet curves under all conditions; however, samples treated with anle138b during fibril formation displayed reduced signal intensity. We interpret this as reflecting a reduction in fibril quantity rather than structural alterations in the fibrils themselves.

L1 A $\beta_{40}$  fibril structure contains an extended loop region (Ala21-Gly33) between  $\beta$ 2 and  $\beta$ 3, comprising non-canonical structural elements such as  $\beta$ -turns and loops. Recent literature<sup>1</sup> (DichroIDP, 2023) suggests that accurate quantitative secondary structure analysis by conventional CD deconvolution methods is challenging for

proteins containing such non-canonical structures. Moreover, Khrapunov (2009) reported that CD analysis reliably quantifies secondary structures only for repetitive all- $\alpha$  or canonical all- $\beta$  proteins, whereas non-canonical elements such as  $\beta$ -turns, loops, or distorted  $\beta$ -strands can lead to misleading interpretations<sup>2</sup>.

Given these structural characteristics of our fibrils and the presence of non-canonical  $\beta$ -turns and loops, we decided against performing secondary structure deconvolution of the CD spectra in this study. We have also revised the main text (lines 112–119, highlighted in blue) to clarify this point.

**Lines 109-120:** CD spectra showed  $\beta$ -sheet signatures under all conditions at the beginning of incubation after mixing A $\beta$ <sub>40</sub> with DMPG liposomes (Supplementary Fig. 1b), indicating similar initial secondary structures regardless of the presence of anle138b. After 48 hours of incubation, a strong  $\beta$ -sheet signal was retained in the control sample (SMPR = 0), whereas  $\beta$ -sheet formation was reduced in samples treated with anle138b (SMPRs = 0.6 and 1.2). Fibril formation was most reduced at SMPR 1.2, notably, indicating a dose dependence (Supplementary Fig. 1a, c). These results were further supported by two complementary approaches performed on a dedicated fibril sample (pre-treatment, post-treatment, control fibril): 1D (<sup>1</sup>H)<sup>15</sup>N CP spectrum signal intensity, and quantification of fibrils by negative stain EM and CD spectroscopy (Fig. 1b, c, Supplementary Fig. 3). All three methods consistently indicated a dose-dependent inhibition of fibril formation by anle138b.

1. Miles, A. J., Drew, E. D., & Wallace, B. A. (2023). DichroIDP: a method for analyses of intrinsically disordered proteins using circular dichroism spectroscopy. *Communications Biology*, 6(1), 823.
2. Khrapunov, S. (2009). Circular dichroism spectroscopy has intrinsic limitations for protein secondary structure analysis. *Analytical biochemistry*, 389(2), 174-176.

**(5) NMR results (Fig. 1C) show a marked reduction in fibrillar signal upon Anle138b treatment in the pre-treatment condition, suggesting reduced fibril formation. In contrast, ssNMR in Fig.3 indicates that the compound can bind within the fibril core. These findings seem partially contradictory. Does Anle138b destabilize early fibril formation but remain stably bound in the formed fibril? Could the central binding pocket identified in figure 3 also play a role in modulating primary nucleation? Further discussion on how the structural data correlate with the dissolution or prevention of fibril formation would be valuable.**

At the current stage, it is difficult to definitively conclude that anle138b directly affects primary nucleation via interaction with the central cavity, based solely on structural data obtained from mature fibrils. It remains possible that anle138b occupies the central cavity during the fibril formation process, or alternatively, inserts into pre-formed fibrils. To explore this possibility, we examined the post-treatment condition, in which anle138b was added to pre-formed L1 A $\beta$ <sub>40</sub> fibrils and incubated for 1 hour. Under these conditions, ssNMR analysis did not provide conclusive evidence of anle138b insertion into the central cavity. These results suggest that compound insertion may vary depending on the timing of exposure during the fibril formation process. This

apparent dual mode of action is further discussed in the final section of the Discussion (lines 403–414), where we propose that anle138b both inhibits early-stage aggregation and selectively binds to mature fibrils.

**Lines 403-414:** Our results reveal a dual mode of action: inhibition of fibril formation during early aggregation and selective binding to mature fibrils without major structural disruption. From a thermodynamic perspective, it is intriguing that anle138b can stably associate with fibrils while simultaneously impeding their formation. Although the structural basis for the observed inhibition remains unresolved, one plausible explanation is that anle138b preferentially stabilizes early, non-fibrillar aggregates, thereby reducing the formation of mature fibrils. This mechanism is similar to that proposed for anle145c, a structurally related diphenyl-pyrazole (DPP) compound, which has been shown to inhibit hIAPP fibrillation and has been proposed to stabilize non-toxic oligomeric species through a thermodynamically driven process<sup>68</sup>. Moving forward, we aim to identify and structurally characterize these compound-stabilized early intermediates, which may hold the key to understanding the therapeutic mechanism of anle138b.

**(6) To reinforce the functional relevance of the identified binding site, the authors might consider performing mutagenesis on key residues within the cavity (e.g., glycine or isoleucine residues) and assessing the effect on compound binding and fibril dissolution. This would provide mechanistic support for the role of the binding pocket in compound action against fibril formation.**

We appreciate the reviewer's insightful suggestion. We agree that site-directed mutagenesis of residues within the cavity, such as glycine or isoleucine, could provide mechanistic insight into the functional role of the binding pocket. However, introducing mutations at these positions may perturb the overall fibril architecture, complicating the interpretation of binding-specific effects. As our study focused on structural and biophysical characterization of anle138b binding, mutational validation was beyond its current scope. Nonetheless, we consider this a promising direction for future work to further elucidate the contribution of individual residues to compound binding and fibril modulation.

**(7) The conclusion that Anle138b competes with ThT for binding may be premature. ThT fluorescence can be influenced by multiple factors, including fibril structure and accessibility. To confirm direct competition, the authors could fix the compound concentration and titrate increasing amounts of ThT to observe potential displacement effects. Such data would help validate this claim.**

We appreciate the reviewer's valuable comments. In response, we have revised the relevant section to present a more cautious interpretation of the observed ThT fluorescence reduction. As the primary focus of this study was to characterize the interaction between anle138b and A $\beta$ <sub>40</sub> fibrils, the ThT signal decrease was treated

as a secondary observation. Similar reductions have been reported in previous studies involving small molecules and amyloid fibrils (as cited in the manuscript) and are not unique to our system.

We acknowledge that reduced ThT fluorescence may reflect changes in fibril structure or dye accessibility following compound binding, rather than direct competition. The reviewer's suggestion to titrate ThT under fixed compound concentration is a sound experimental approach for clarifying this mechanism and represents an important direction for future studies.

The manuscript has been revised to reflect the reviewer's comments as follows (135-139, highlighted in blue):

**Lines 134-140:** The observed reduction in ThT fluorescence intensity in the post-treatment sample (the fibril treated with anle138b after their formation) is likely attributable to competitive binding between anle138b and ThT at shared or nearby fibril binding sites. Thus, the fluorescence intensity cannot be used as a measure of fibril quantity, and complementary readouts suggest that the fibril quantity has not decreased significantly (Fig. 1b, c, Supplementary Fig. 3b). This interpretation is consistent with previously reported interactions between small molecules and amyloid fibrils<sup>21,22</sup>.

**(8) In the ITC experiments, the compound is solubilized in DLPG. It is unclear, however, whether the A $\beta$  fibrils used in these experiments (post-treatment) were also prepared in DLPG or in a different lipid or buffer system. Since pre- and post-treatment experiments involve different lipids (DMPG vs. DLPG), this could affect the comparability of binding data and should be clarified.**

We thank the reviewer for this important comment. As addressed in our response to Reviewer comments 2, the pre-formed fibrils used in both the ITC experiments and the post-treatment condition were generated in the presence of DMPG liposomes, under the same conditions as the control fibrils. This clarification is also reflected in the revised manuscript (*lines 125–126, highlighted in blue*).

We note that this point overlaps with Reviewer #2's earlier comments.

DLPG vesicles were used solely as delivery vehicles for anle138b in the post-treatment and ITC experiments and were not involved in fibril formation. Importantly, no detectable interaction between DLPG and the fibrils was observed by ITC, ssNMR, or cryo-EM. These combined results confirm that the binding data most likely reflect direct interactions between anle138b and DMPG-based fibrils, without confounding effects from lipid composition.

**(9) The authors apply a flat-bottomed positional restraint in their MD simulations. More explanation is needed regarding the purpose of this restraint and whether it might limit**

**the natural flexibility of the compound-fibril interaction. Could this influence the binding mode or energetics observed?**

Since Reviewer 2 also commented on this, we added further explanation to the MD simulation methods section, with the relevant details [highlighted in blue](#).

When the molecule is within the flat bottom of the positional potential, the potential imposes no force on the molecule. The protein atoms of all residues in or around the central cavity are also not restrained. We therefore expect no influence on the compound-fibril interaction. Consequently, if we restrict our consideration to the cavity binding modes, then there should be no influence on the observed binding modes. Similar arguments apply for energetics. Of course, we cannot compare the results to surface binding, nor do we propose to compute binding affinities.

In more detail, the flat-bottomed restraint keeps the ligand within a cylinder above the central cavity of the L1 between the two protofilaments of the L1 A $\beta$ <sub>40</sub> fibril, thereby preventing it from diffusing away, and increasing the probability that the molecule encounters the cavity opening. This is crucial for observing the (otherwise unsteered or unbiased) probing and binding of the ligand to and into the central cavity within reasonable simulation times. The cylinder is chosen large enough to allow the molecule to rotate and orient freely above the central cavity (radius cylinder ~ longest extension of the molecule, see Supplementary Figure 24). As mentioned, the flat-bottomed positional restraint does influence the observed binding mode insofar as it restricts the conformational space available to the ligand to a cylindrical volume. If other, perhaps more stable or transient, binding modes exist outside the restricted volume, they are not observed with this set of simulations alone. However, these simulations were necessary to complement the wider range of alternative anle138b poses observed in the simulations with multiple ligands without restraints, since the limited sampling without restraints is insufficient to investigate the slower on-rates associated with cavity binding. The goal of the simulations of truncated fibril models with flat-bottomed positional restraints is primarily to show the *principal/general* ability of the ligand to bind into the central cavity and to record the interatomic protein-ligand distances while doing so. See also reply to comments (4) of **Reviewer #2 on p. 8-10**.

**Reviewer #4 (Remarks to the Author):**

I co-reviewed this manuscript with one of the reviewers who provided the listed reports. This is part of the Nature Communications initiative to facilitate training in peer review and to provide appropriate recognition for Early Career Researchers who co-review manuscripts.

## REVIEWER COMMENTS

### Reviewer #2 (Remarks to the Author):

I appreciate the authors' responsiveness and clarity. However, their revisions leave a couple of issues that I believe still need to be addressed:

**1. I was confused by the rationale that that DLPG was selected to reduce charge-based nonspecific interactions, given that DLPG and DMPG have the same head group and charge state. The subsequent parallel rationale based on membrane phase and fluidity, while speculative, is clearer and more plausible.**

Thank you for your comment.

We agree that the explanation stating DLPG was selected due to differences in charge state may be confusing. This sentence has been removed from the manuscript. Instead, we now explain the use of DLPG based on its lower melting temperature ( $T_m = -3\text{ }^{\circ}\text{C}$ ), which maintains high membrane fluidity at  $25\text{ }^{\circ}\text{C}$  and facilitates the dispersion of hydrophobic compounds such as anle138b.

**2. The initial version of the manuscript clearly explained that the DLPG is likely to be in a micelle-like state and is referred to as 'vesicles' only for convenience. This is an essential disclosure that has been lost in the revision, and I believe it needs to be added back to the manuscript.**

In response to your comment, we have reinserted the explanation regarding the physical state of DLPG in the Methods section. DLPG is likely to adopt a micelle-like structure under the experimental conditions used, and the term 'vesicle' is used merely as a convenient descriptor to simplify the description of the system.

**Both points you raised have been addressed in the Methods section, highlighted in purple for clarity.**

For post-treatment fibril, DLPG lipid films containing anle138b were hydrated and sonicated for 15 minutes in 10 mM sodium phosphate buffer (pH 6.5), yielding lipid-based particles <10 nm in diameter to solubilize the hydrophobic compound. Although the exact structural identity of DLPG particles remains unclear, with their small size (<10 nm) and physicochemical properties suggesting they are more likely micelles, non-bilayer structures, or ultrasmall unilamellar vesicles<sup>81</sup>, we refer to them as vesicles throughout this work for clarity. For post-treatment conditions, DLPG vesicles were used to deliver anle138b to pre-formed L1 A $\beta$ <sub>40</sub> fibrils. DLPG was selected over DMPG due to its lower melting temperature ( $T_m = -3\text{ }^{\circ}\text{C}$ ), which ensures high membrane fluidity at 25 °C and facilitates dispersion of hydrophobic molecules such as anle138b. To minimize co-sedimentation artifacts during centrifugation, small unilamellar DLPG vesicles were used. Control ITC experiments confirmed that DLPG vesicles alone exhibited no measurable binding enthalpy with L1 A $\beta$ <sub>40</sub> fibrils, supporting their role as a passive solubilizing vehicle for anle138b.



Reporting Summary

Nature Portfolio wishes to improve the reproducibility of the work that we publish. This form provides structure for consistency and transparency in reporting. For further information on Nature Portfolio policies, see our [Editorial Policies](#) and the [Editorial Policy Checklist](#).

Statistics

For all statistical analyses, confirm that the following items are present in the figure legend, table legend, main text, or Methods section.

n/a	Confirmed
<input type="checkbox"/>	<input checked="" type="checkbox"/> The exact sample size ( <i>n</i> ) for each experimental group/condition, given as a discrete number and unit of measurement
<input type="checkbox"/>	<input checked="" type="checkbox"/> A statement on whether measurements were taken from distinct samples or whether the same sample was measured repeatedly
<input checked="" type="checkbox"/>	<input type="checkbox"/> The statistical test(s) used AND whether they are one- or two-sided <i>Only common tests should be described solely by name; describe more complex techniques in the Methods section.</i>
<input checked="" type="checkbox"/>	<input type="checkbox"/> A description of all covariates tested
<input checked="" type="checkbox"/>	<input type="checkbox"/> A description of any assumptions or corrections, such as tests of normality and adjustment for multiple comparisons
<input type="checkbox"/>	<input checked="" type="checkbox"/> A full description of the statistical parameters including central tendency (e.g. means) or other basic estimates (e.g. regression coefficient) AND variation (e.g. standard deviation) or associated estimates of uncertainty (e.g. confidence intervals)
<input checked="" type="checkbox"/>	<input type="checkbox"/> For null hypothesis testing, the test statistic (e.g. <i>F</i> , <i>t</i> , <i>r</i> ) with confidence intervals, effect sizes, degrees of freedom and <i>P</i> value noted <i>Give P values as exact values whenever suitable.</i>
<input checked="" type="checkbox"/>	<input type="checkbox"/> For Bayesian analysis, information on the choice of priors and Markov chain Monte Carlo settings
<input checked="" type="checkbox"/>	<input type="checkbox"/> For hierarchical and complex designs, identification of the appropriate level for tests and full reporting of outcomes
<input checked="" type="checkbox"/>	<input type="checkbox"/> Estimates of effect sizes (e.g. Cohen's <i>d</i> , Pearson's <i>r</i> ), indicating how they were calculated

Our web collection on [statistics for biologists](#) contains articles on many of the points above.

Software and code

Policy information about [availability of computer code](#)

Data collection	NMR: Bruker TopSpin(V3.6.5 and V4) Cryo-EM :SerialEM(V4.0) MD simulations: GROMACS 2023 (including implementations of P-LINCS, SETTLE, non-bonded Verlet scheme, PME, velocity-rescale Temperature coupling and Parrinello-Rahman barostat).
Data analysis	NMR data : CcpNMR(V 2.4.2), TopSpin(V 3.6.5). ITC data : MicroCal control software. Cryo-EM data : RELION(V3.1), CTFFIND(V4.1), COOT(V0.9), PHENIX(V1.19). MD simulations: Awk and Bash scripts were used to postprocess output from GROMACS 2023 analysis tools (gmx mindist and gmx traj) and g_contacts (Blau et.al.) used to calculate interatomic distances. Visualisation of fibril structure : Chimera(V1.8), ChimeraX(V1.9), Pymol

For manuscripts utilizing custom algorithms or software that are central to the research but not yet described in published literature, software must be made available to editors and reviewers. We strongly encourage code deposition in a community repository (e.g. GitHub). See the Nature Portfolio [guidelines for submitting code & software](#) for further information.

## Data

Policy information about [availability of data](#)

All manuscripts must include a [data availability statement](#). This statement should provide the following information, where applicable:

- Accession codes, unique identifiers, or web links for publicly available datasets
- A description of any restrictions on data availability
- For clinical datasets or third party data, please ensure that the statement adheres to our [policy](#)

NMR spectra raw data generated in this study of Amyloid beta (1-40) fibrils has been deposited in the BMRB under accession number 53129.

MD simulation input files, final coordinate files, and raw trajectory data generated in this study have been deposited in the Edmond data repository (<https://doi.org/10.17617/3.NRYUVQ>). Cryo-EM density maps and atomic models of L1 Aβ40 fibrils (both pre- and post-treatment fibril) have been deposited in the EMDB (EMD-53882 and EMD-53880) and PDB (9RAX and 9RAW).

## Research involving human participants, their data, or biological material

Policy information about studies with [human participants or human data](#). See also policy information about [sex, gender \(identity/presentation\), and sexual orientation](#) and [race, ethnicity and racism](#).

Reporting on sex and gender	Not applicable
Reporting on race, ethnicity, or other socially relevant groupings	Not applicable
Population characteristics	Not applicable
Recruitment	Not applicable
Ethics oversight	Not applicable

Note that full information on the approval of the study protocol must also be provided in the manuscript.

## Field-specific reporting

Please select the one below that is the best fit for your research. If you are not sure, read the appropriate sections before making your selection.

- ☒ Life sciences ☐ Behavioural & social sciences ☐ Ecological, evolutionary & environmental sciences

For a reference copy of the document with all sections, see [nature.com/documents/nr-reporting-summary-flat.pdf](https://www.nature.com/documents/nr-reporting-summary-flat.pdf)

## Life sciences study design

All studies must disclose on these points even when the disclosure is negative.

Sample size	<p>Fibril preparation and characterization: Fibril samples were prepared and initially assessed by negative-stained electron microscopy (EM) to confirm fibril formation. Structural reproducibility was evaluated by solid-state NMR experiments (hCANH, hNCA, <math>^{13}\text{C}</math>-<math>^{13}\text{C}</math> DARR, <math>^{13}\text{C}</math>-<math>^{13}\text{C}</math> RFDR, and NHH) using differently labeled fibrils: uniformly labeled with <math>^{13}\text{C}</math>, uniformly labeled with <math>^{13}\text{C}</math> and <math>^{15}\text{N}</math>, perdeuterated (<math>^2\text{H}</math>, <math>^{13}\text{C}</math>, <math>^{15}\text{N}</math>), and selectively labeled with <math>^{13}\text{C}</math>, <math>^{15}\text{N}</math> at Lys and Ile residues.</p> <p>NMR experiments: The number of scans was adjusted based on the signal-to-noise ratio (S/N). Data acquisition was continued until sufficient S/N was achieved.</p> <p>Cryo-EM data acquisition: Cryo-EM data were collected for both pre-treatment and post-treatment conditions. The datasets comprised 21,576 micrographs for the pre-treatment fibrils and 7,311 micrographs for the post-treatment fibrils. Cryo-EM, NMR, and negative-stain EM measurements were all performed on the <math>^1\text{H}</math>, <math>^{13}\text{C}</math>, <math>^{15}\text{N}</math>-labeled fibril sample.</p> <p>MD simulations: a total of 20 MD simulations of anle138b binding to the fibril surface and the central fibril cavity were run for 250 to 1000 ns, respectively.</p>
Data exclusions	<p>No NMR data were excluded from the analysis.</p> <p>Standard image classification procedures were employed to select particle images for high-resolution reconstructions, following established protocols (Scheres, J. Struct. Biol. 180, 519–530 (2021)). Details on the number of selected images are provided in Supplementary Table S3.</p>
Replication	<p>During fibril formation, samples were monitored using Thioflavin T (ThT) fluorescence, circular dichroism (CD) spectroscopy, and solid-state NMR (hCANH and hNH) experiments.</p> <p>The protocol was repeated three times using differently labeled NMR samples (<math>^1\text{H}^{13}\text{C}^{15}\text{N}</math>, <math>^2\text{H}^{13}\text{C}^{15}\text{N}</math>, <math>^{13}\text{C}</math>, and <math>^{13}\text{C}^{15}\text{N}</math> Lys- or Ile-selectively labeled), consistently yielding identical spectra in both hCANH and hNH experiments.</p> <p>Cryo-EM samples were validated using ThT fluorescence, CD spectroscopy, negative-stain EM, and NMR to confirm structural consistency with the fibril samples.</p> <p>MD simulations: in all, for the different binding modes (fibril surface: with and without lipids; central cavity; protonated and unprotonated lysine 28), 40 simulations were run. Each condition was run between five to ten independent production simulations.</p>

Randomization

Randomization was not performed for the both methods (ssNMR and Cryo-EM).

Blinding

Blinding was not applied for NMR experiments, as adjustment of experimental parameters requires prior knowledge of the isotope labeling scheme. Improper parameter settings could significantly increase measurement times, which range from several days to weeks.

Blinding was also not implemented for cryo-EM, as the risk of experimental bias was assessed to be minimal given the objective nature of image acquisition and particle selection procedures.

## Reporting for specific materials, systems and methods

We require information from authors about some types of materials, experimental systems and methods used in many studies. Here, indicate whether each material, system or method listed is relevant to your study. If you are not sure if a list item applies to your research, read the appropriate section before selecting a response.

### Materials & experimental systems

n/a	Involved in the study
<input checked="" type="checkbox"/>	<input type="checkbox"/> Antibodies
<input checked="" type="checkbox"/>	<input type="checkbox"/> Eukaryotic cell lines
<input checked="" type="checkbox"/>	<input type="checkbox"/> Palaeontology and archaeology
<input checked="" type="checkbox"/>	<input type="checkbox"/> Animals and other organisms
<input checked="" type="checkbox"/>	<input type="checkbox"/> Clinical data
<input checked="" type="checkbox"/>	<input type="checkbox"/> Dual use research of concern
<input checked="" type="checkbox"/>	<input type="checkbox"/> Plants

### Methods

n/a	Involved in the study
<input checked="" type="checkbox"/>	<input type="checkbox"/> ChIP-seq
<input checked="" type="checkbox"/>	<input type="checkbox"/> Flow cytometry
<input checked="" type="checkbox"/>	<input type="checkbox"/> MRI-based neuroimaging

## Plants

Seed stocks

Not applicable

Novel plant genotypes

Not applicable

Authentication

Not applicable

## **Supplemental Information**

### **Anle138b binds predominantly to the central cavity in lipidic A $\beta$ <sub>40</sub> fibrils and modulates fibril formation.**

Mookyoung Han<sup>1</sup>, Benedikt Frieg<sup>2</sup>, Dirk Matthes<sup>3</sup>, Andrei Leonov<sup>1,4</sup>, Sergey Ryazanov<sup>1,4</sup>, Karin Giller<sup>1</sup>, Evgeny Nimerovsky<sup>1</sup>, Marianna Stampolaki<sup>1</sup>, Kai Xue<sup>1</sup>, Kerstin Overkamp<sup>1</sup>, Christian Dienemann<sup>5</sup>, Dietmar Riedel<sup>6</sup>, Armin Giese<sup>4</sup>, Stefan Becker<sup>1</sup>, Bert L. de Groot<sup>3</sup>, Gunnar F. Schröder<sup>2,7</sup>, Loren B. Andreas<sup>1\*</sup> and Christian Griesinger<sup>1,8\*</sup>

<sup>1</sup>. Department of NMR-Based Structural Biology, Max Planck Institute for Multidisciplinary Sciences, Göttingen, Germany.

<sup>2</sup>. Ernst-Ruska Centre for Microscopy and Spectroscopy with Electrons, ER-C-3 Structural Biology, Forschungszentrum Jülich, Jülich, Germany

<sup>3</sup>. Department of Theoretical and Computational Biophysics, Max Planck Institute for Multidisciplinary Sciences; Göttingen, Germany.

<sup>4</sup>. MODAG GmbH, Mikroforum Ring 3, 55234, Wendelsheim, Germany

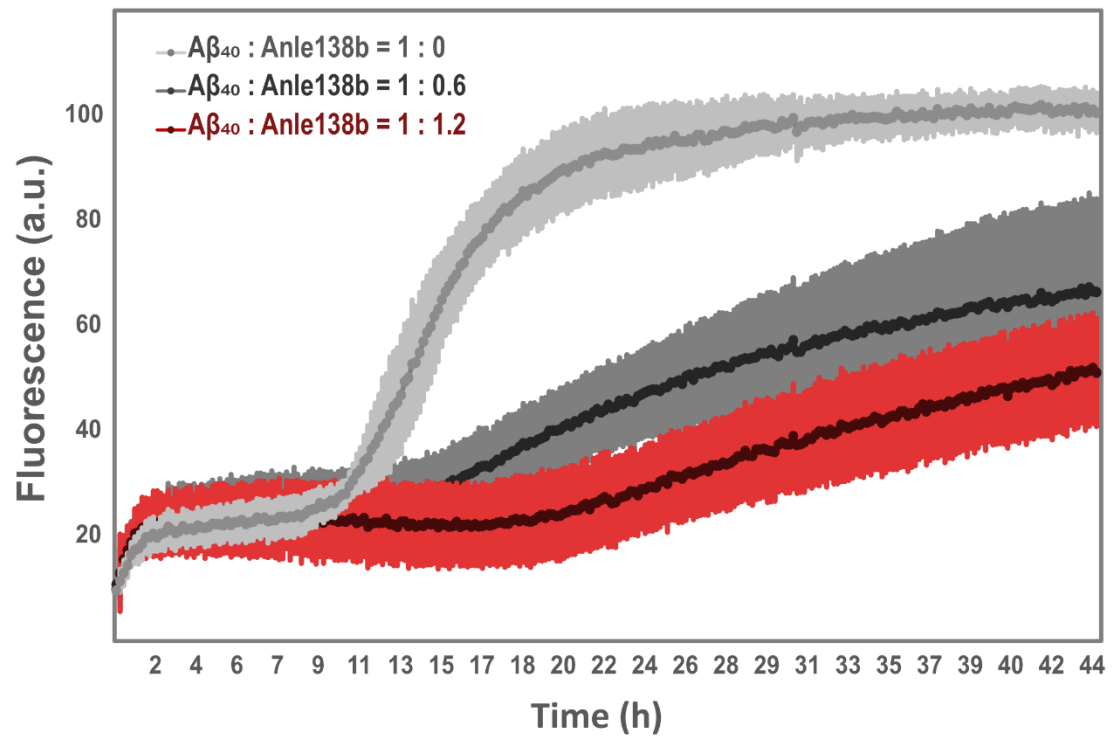
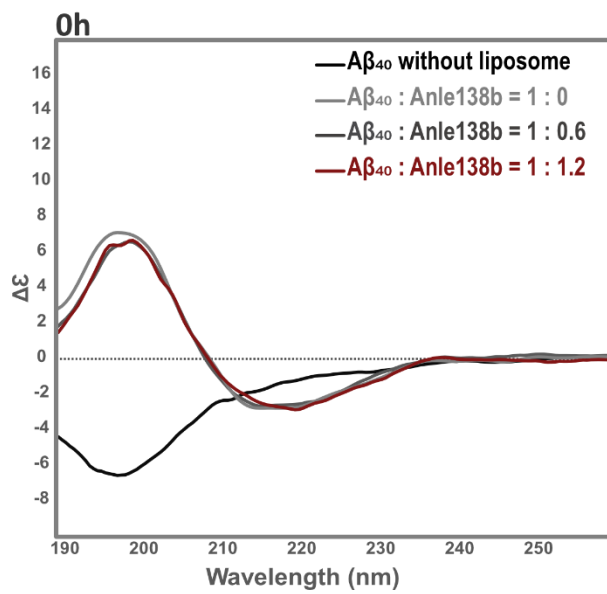
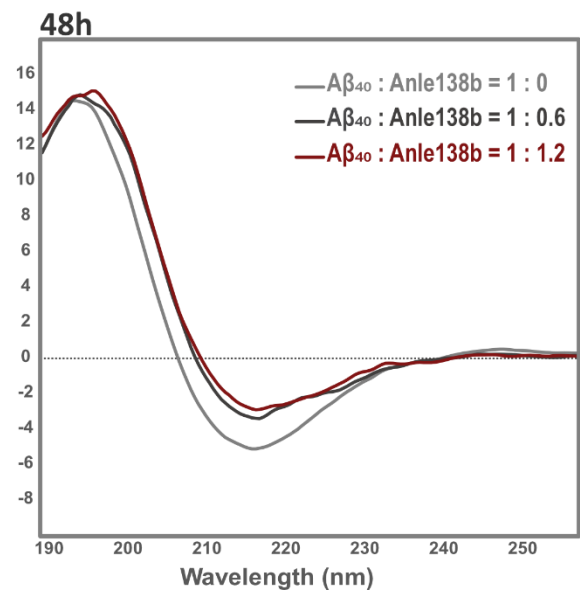
<sup>5</sup>. Department of Molecular Biology, Max Planck Institute for Multidisciplinary Sciences, Göttingen, Germany.

<sup>6</sup>. Laboratory of Electron Microscopy, Max-Planck-Institute for Multidisciplinary Sciences, Göttingen, Germany.

<sup>7</sup>. Physics Department, Heinrich Heine University Düsseldorf; Düsseldorf, Germany

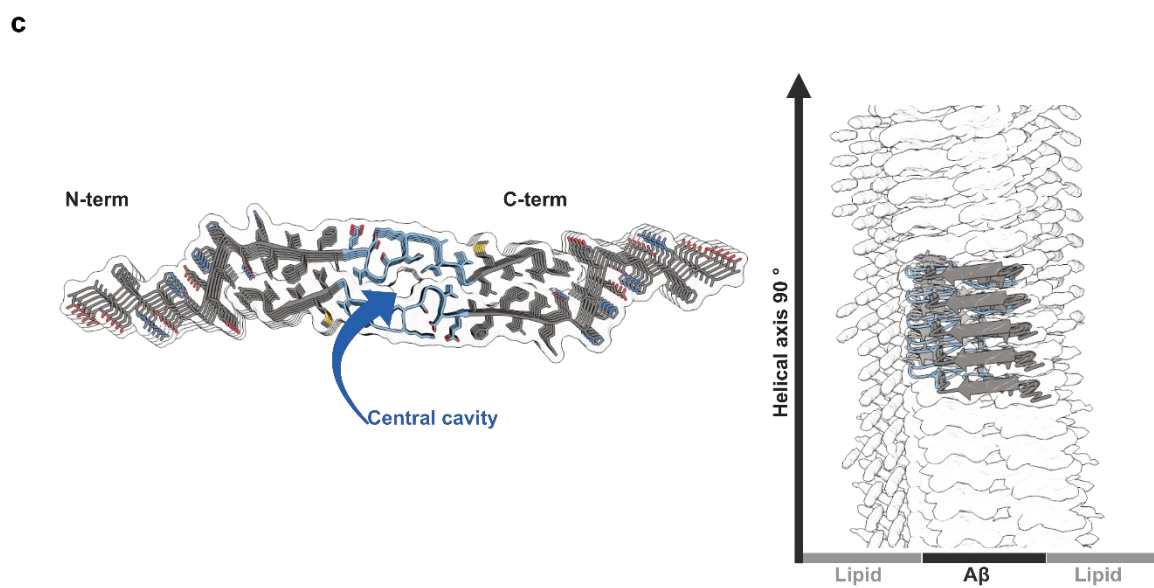
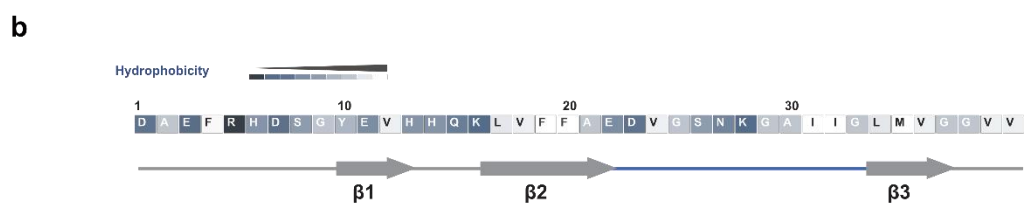
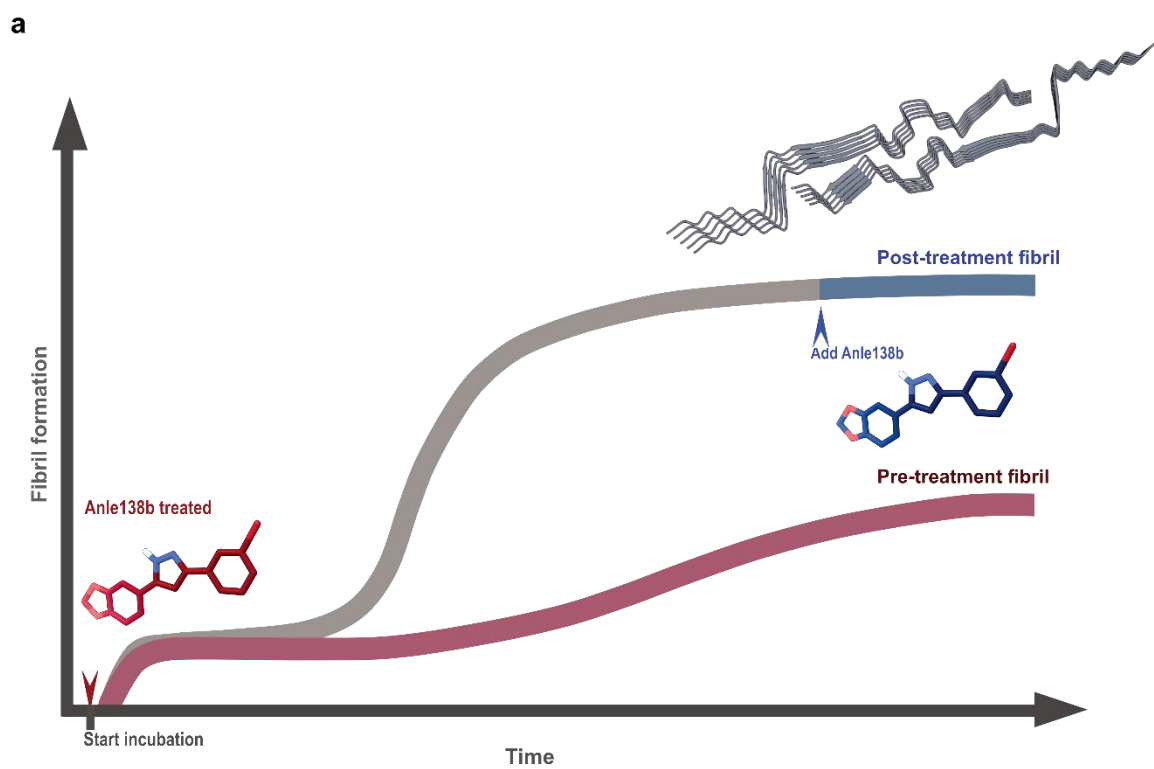
<sup>8</sup>. Cluster of Excellence "Multiscale Bioimaging: From Molecular Machines to Networks of Excitable Cells" (MBExC), University of Göttingen; Göttingen, Germany.

\* Correspondence and requests for materials should be addressed to Loren B. Andreas (land@mpinat.mpg.de) and Christian Griesinger (cigr@mpinat.mpg.de).

**a****b****c**

**Supplementary Figure 1 | Anle138b modulates L1 A $\beta$ <sub>40</sub> fibril formation and secondary structure under the pre-treatment condition.**

**a.** The ThT fluorescence assay shows the effect of increasing concentrations of anle138b on A $\beta$ <sub>40</sub> fibril formation. The control fibrils (anle138b: A $\beta$ <sub>40</sub> molar ratio (SMPR) = 0) are shown in light gray, the intermediate concentration (SMPR = 0.6) in dark gray, and the high concentration (SMPR = 1.2) in red. At the highest concentration, anle138b extends the lag phase by approximately 8–10 hours and reduces the overall ThT fluorescence intensity by 40–60%. Fluorescence intensity is shown in arbitrary units (a.u.). Curves show mean fluorescence, with shaded areas indicating mean  $\pm$  s.d. (n = 6 biological replicates, each from independently prepared A $\beta$ <sub>40</sub> samples purified from separate expression batches). **b.** Circular dichroism (CD) spectra acquired at 0 hours show  $\beta$ -sheet formation in all conditions (SMPR = 0, 0.6, and 1.2; light gray, dark gray, red). No significant differences were observed between the formation of the  $\beta$ -sheet in the presence or absence of anle138b. **c.** CD spectra after 48 hours of incubation reveal strong  $\beta$ -sheet content in the control fibrils (light gray), while fibrils treated with anle138b (dark gray for SMPR = 0.6, red for SMPR = 1.2) exhibit reduced  $\beta$ -sheet formation. Source data are provided as a Source Data file.



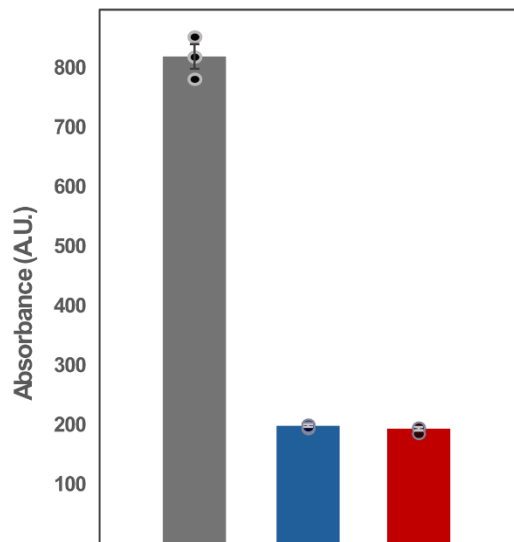
## **Supplementary Figure 2 | Schematic illustration of experiments investigating the binding sites of anle138b on L1 A $\beta$ <sub>40</sub> fibrils.**

**a.** Schematic illustration of L1 A $\beta$ <sub>40</sub> fibril formation under pre-treatment and post-treatment conditions. In the post-treatment condition, anle138b (blue) is added after fibril formation. In the pre-treatment condition, fibrils form in the presence of anle138b (red), which extends the lag phase and reduces the final fibril amount. The two arrows indicate the time points at which anle138b was administered during the fibril formation process. Blue represents the post-treatment condition, and red represents the pre-treatment condition. This schematic provides a conceptual overview of the experimental timeline and administration of anle138b, complementing the corresponding kinetic data shown in Supplementary Fig. 1a and Fig. 1c. **b.** Amino acid sequence and secondary structure of the L1 A $\beta$ <sub>40</sub> fibril. Hydrophobicity is color-coded using a gradient from dark blue (hydrophilic) to white (hydrophobic), based on the Eisenberg scale<sup>65</sup>. The loop region (Ala21–Gly33), highlighted in blue, contributes to the formation of the central cavity between the two protofilaments. **c.** Structure of the L1 A $\beta$ <sub>40</sub> fibril based on cryo-EM data. Left: Top view of the fibril showing the loop region (blue); the blue arrow indicates the central cavity. Right: Side view highlighting the periodic alignment of rod-shaped lipid densities along the fibril axis, as visualized in the cryo-EM map.

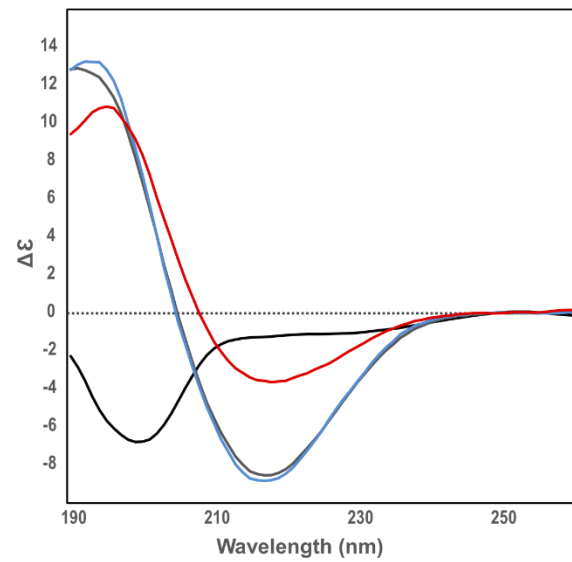


- $A\beta_{40}$  monomer without DMPG liposome
- Control fibril = 1 : 0 ( $A\beta_{40}$  : anle138b)
- Post treatment fibril = 1 : 1.2 ( $A\beta_{40}$  : anle138b)
- Pre treatment fibril = 1 : 1.2 ( $A\beta_{40}$  : anle138b)

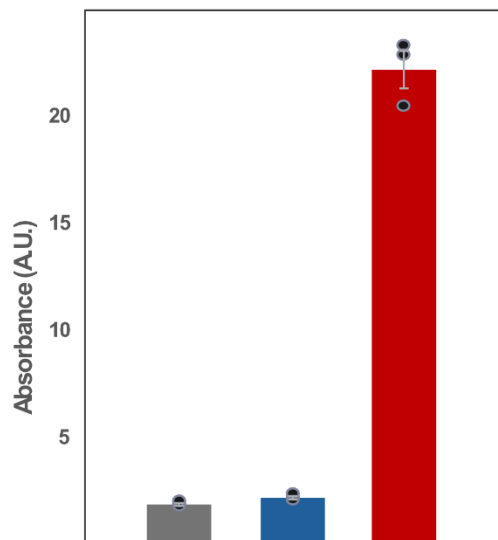
**a**



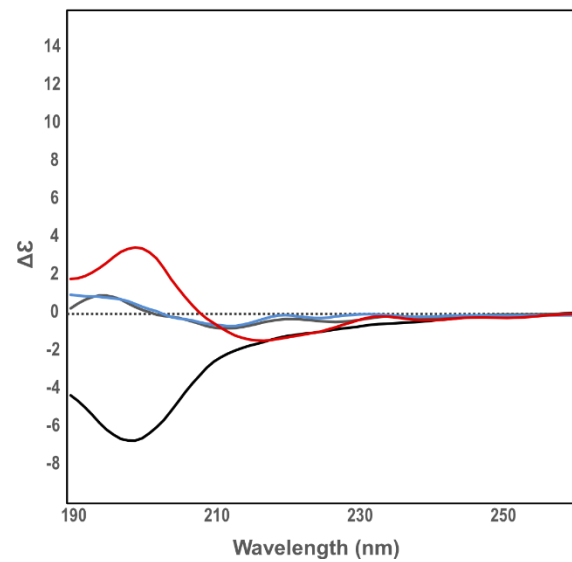
**b**



**c**



**d**

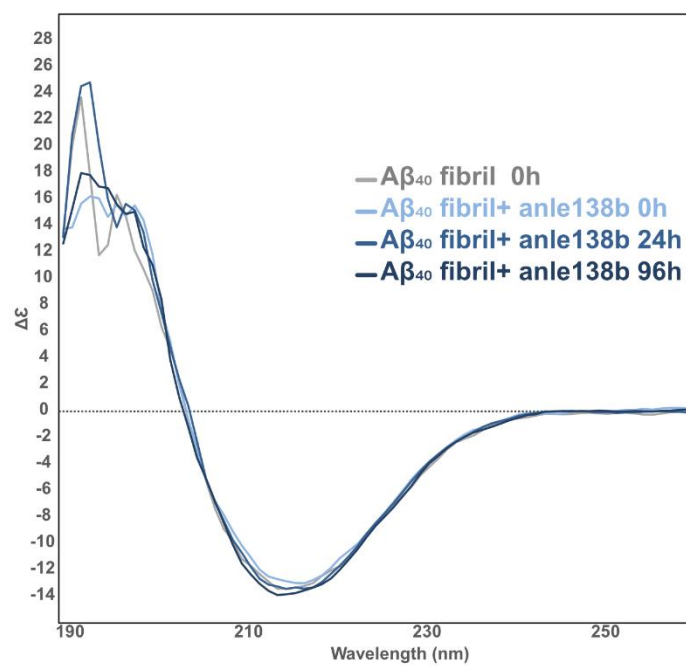


### Supplementary Figure 3 | Effects of anle138b on L1 A $\beta$ <sub>40</sub> fibril formation and structural interaction.

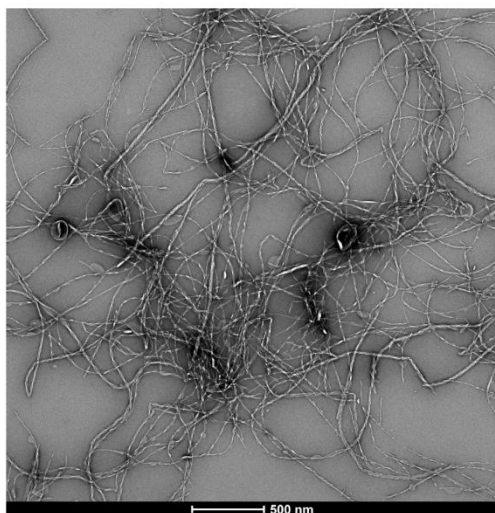
The results shown here were obtained from the same sample sets used for cryo-EM (Fig. 2) as well as in negative-stain EM, 1D (<sup>1</sup>H) <sup>15</sup>N CP NMR experiments (Fig. 1b, c), 2D <sup>13</sup>C/<sup>13</sup>C-DARR spectra (Supplementary Figs. 15, 16), and 2D (H)NCA spectra (Supplementary Fig 5).

**a.** ThT fluorescence assay of L1 A $\beta$ <sub>40</sub> fibrils prepared under three different conditions. The control sample contains (gray) in the absence of anle138b. In the post-treatment condition (blue; anle138b: A $\beta$ <sub>40</sub> molar ratio (SMPR) = 1.2) and in the pre-treatment condition (red; SMPR = 1.2). **b.** CD spectra of L1 A $\beta$ <sub>40</sub> fibrils under the same conditions as in **a**. The control (gray) shows characteristic  $\beta$ -sheet content. The post-treatment condition (blue) exhibits a spectrum similar to the control, indicating that the  $\beta$ -sheet structure is largely preserved. In contrast, the pre-treatment condition (red), where anle138b was present during fibril formation, shows less  $\beta$ -sheet content. A $\beta$ <sub>40</sub> monomer without DMPG liposome (black) **c.** ThT fluorescence assay of the supernatant obtained after ultracentrifugation of the samples prepared as in panel a. In the pre-treatment condition (red), ThT fluorescence was detected in the supernatant, suggesting the presence of non-fibrillar aggregates remaining in solution. **d.** CD spectra of the same supernatant samples analyzed in panel c. The control (gray) and post-treatment (blue) conditions show flat spectra with no significant secondary structure signals, while the pre-treatment condition (red) displays a  $\beta$ -strand-like spectral pattern, indicating the presence of  $\beta$ -strand structures in the non-fibrillar species within the supernatant. The CD spectrum of A $\beta$ <sub>40</sub> monomer without DMPG liposome is shown in black. ThT fluorescence is reported in arbitrary units (a.u.); CD spectra are plotted as  $\Delta\epsilon$ . Bars in a and c show mean  $\pm$  s.e.m. with individual data points overlaid (n = 3, technical replicates from a single sample). Source data are provided as a Source Data file.

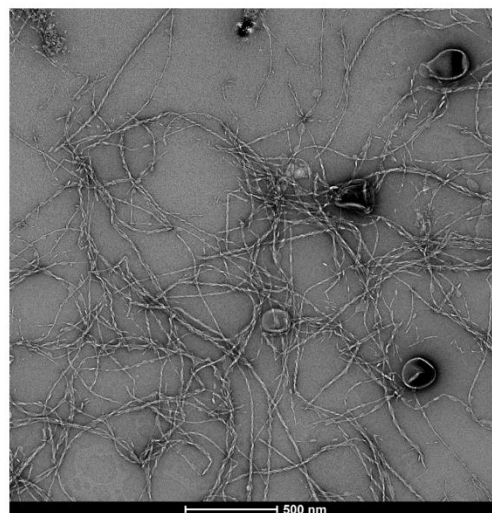
**a**



**b**



**c**

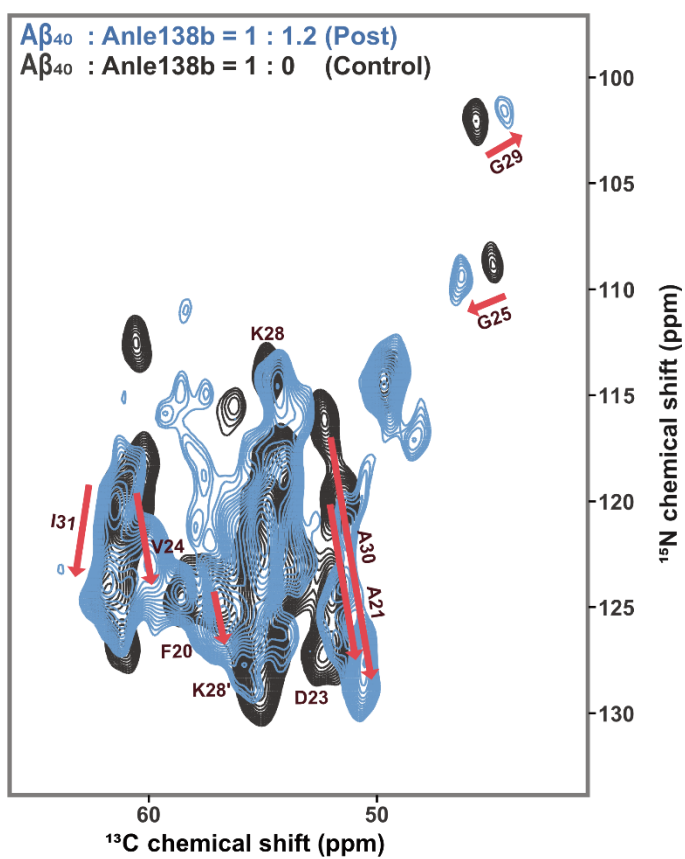


**Supplementary Figure 4 | CD spectroscopy and negative-stain EM analysis of L1 A $\beta$ <sub>40</sub> fibrils under post-treatment condition (anle138b: A $\beta$ <sub>40</sub> molar ratio (SMPR) = 1.2).**

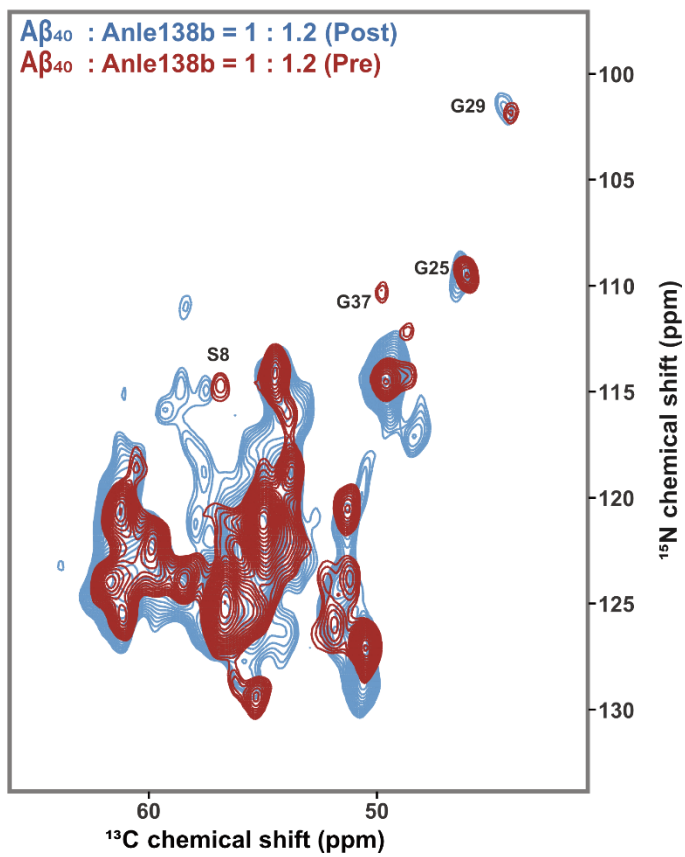
The secondary structure of L1 A $\beta$ <sub>40</sub> fibrils treated with anle138b was assessed by CD spectroscopy under post-treatment conditions, following incubation at 37 °C for up to 96 hours.

**a.** CD spectra of L1 A $\beta$ <sub>40</sub> fibrils at various time points after anle138b addition: untreated (gray, 0 h), immediately after treatment (light blue, 0 h), 24 h (blue), and 96 h (dark blue). Source data are provided as a Source Data file. **b, c.** Negative-stain EM images of L1 A $\beta$ <sub>40</sub> fibrils at 0 h and 96 h after anle138b treatment.

**a**

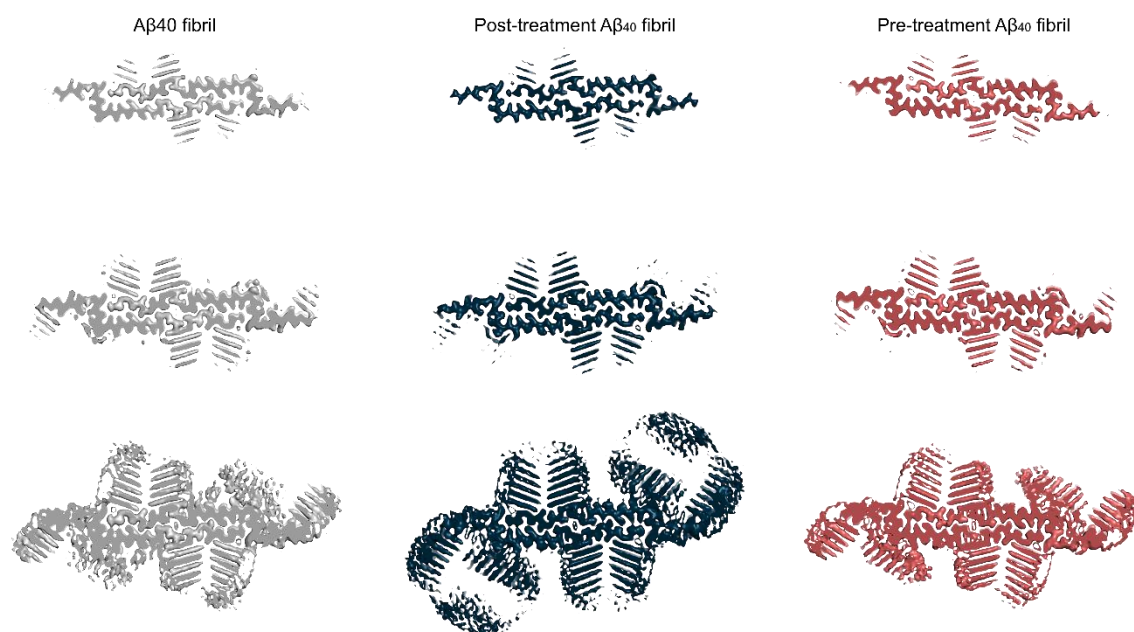


**b**



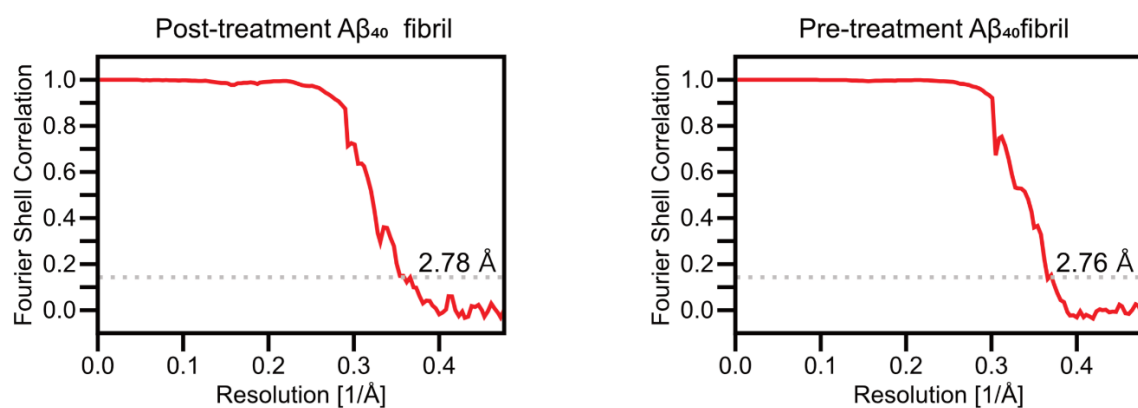
**Supplementary Figure 5 | Superimposed 2D (H)NCA spectra of L1 A $\beta$ <sub>40</sub> fibrils under control, pre-treatment, and post-treatment conditions.**

The spectra were obtained from the same sample sets utilized in cryo-EM (Fig. 2, Supplementary Figs. 6, 7), negative-stain EM, and solid-state NMR experiments (Fig. 1b, c, Supplementary Figs. 15, 16). **a.** Superimposed 2D (H)NCA spectra of L1 A $\beta$ <sub>40</sub> fibrils. The blue spectrum represents fibrils treated with anle138b after fibril formation (post-treatment condition; anle138b: A $\beta$ <sub>40</sub> molar ratio (SMPR) =1.2, ns = 64), while the black spectrum corresponds to fibrils formed in the absence of anle138b (control condition; ns = 64). Chemical shift perturbations induced by anle138b treatment are indicated by pink arrows. **b.** Superimposed 2D (H)NCA spectra comparing the pre- and post-treatment conditions. The red spectrum represents fibrils formed in the presence of anle138b during aggregation (pre-treatment; SMPR 1.2, ns = 192), while the blue spectrum corresponds to the post-treatment condition (SMPR 1.2, ns = 64).



**Supplementary Figure 6 | Sharpened high-resolution maps at different iso-surface levels, L1 Aβ<sub>40</sub> fibrils.**

From the top to the bottom, the iso-surface level threshold decreases such that additional low-resolution features become visible.

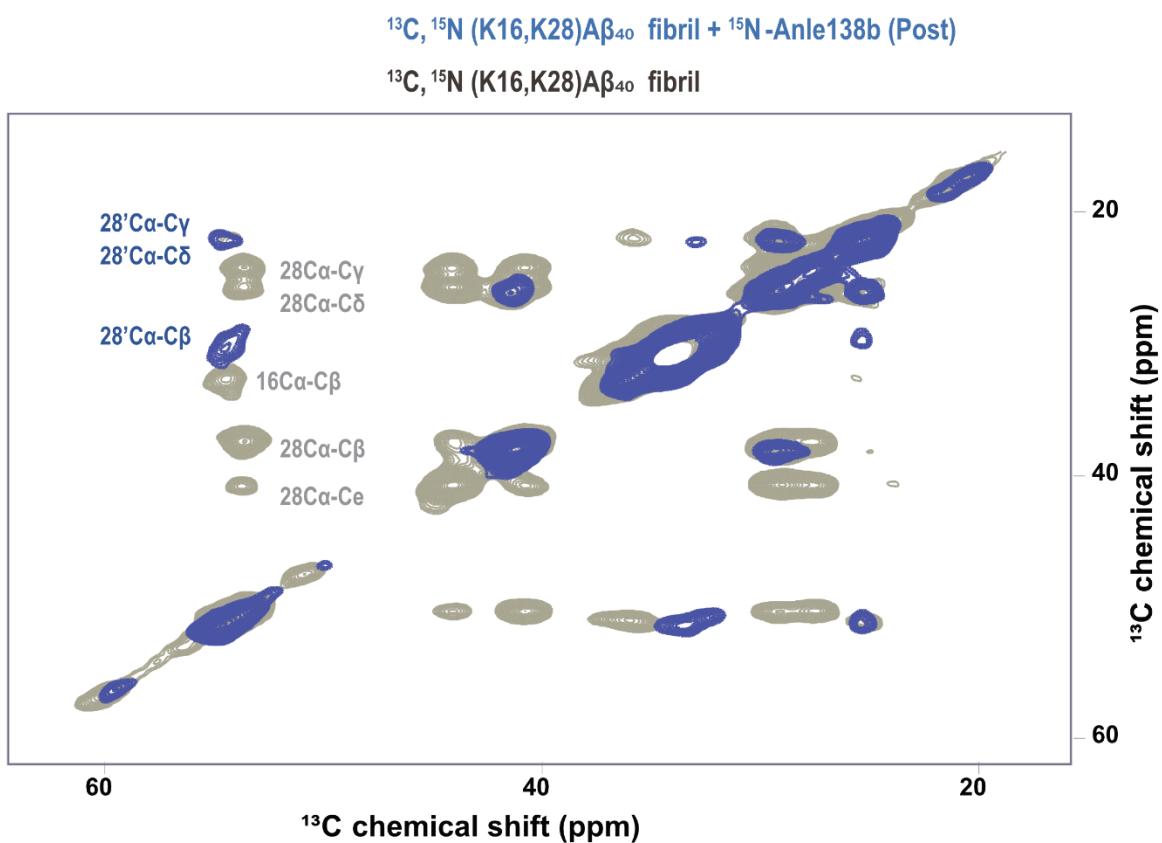


### Supplementary Figure 7 | Fourier shell correlation curves.

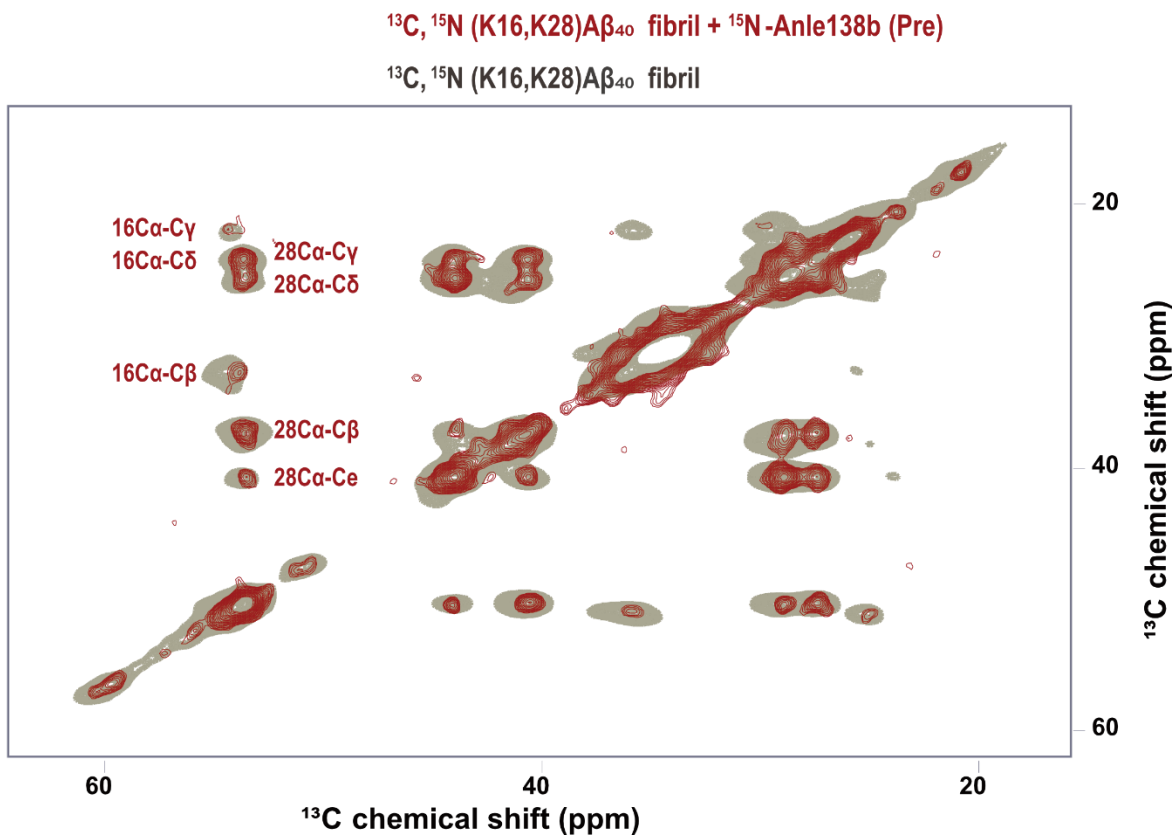
Masked-corrected (z-percentage is 0.1) Fourier shell correlation (FSC) curves. The final resolution is shown in the plot and was estimated from the value of the FSC curve for two separately refined masked half-maps at 0.143 (red line).



**a**



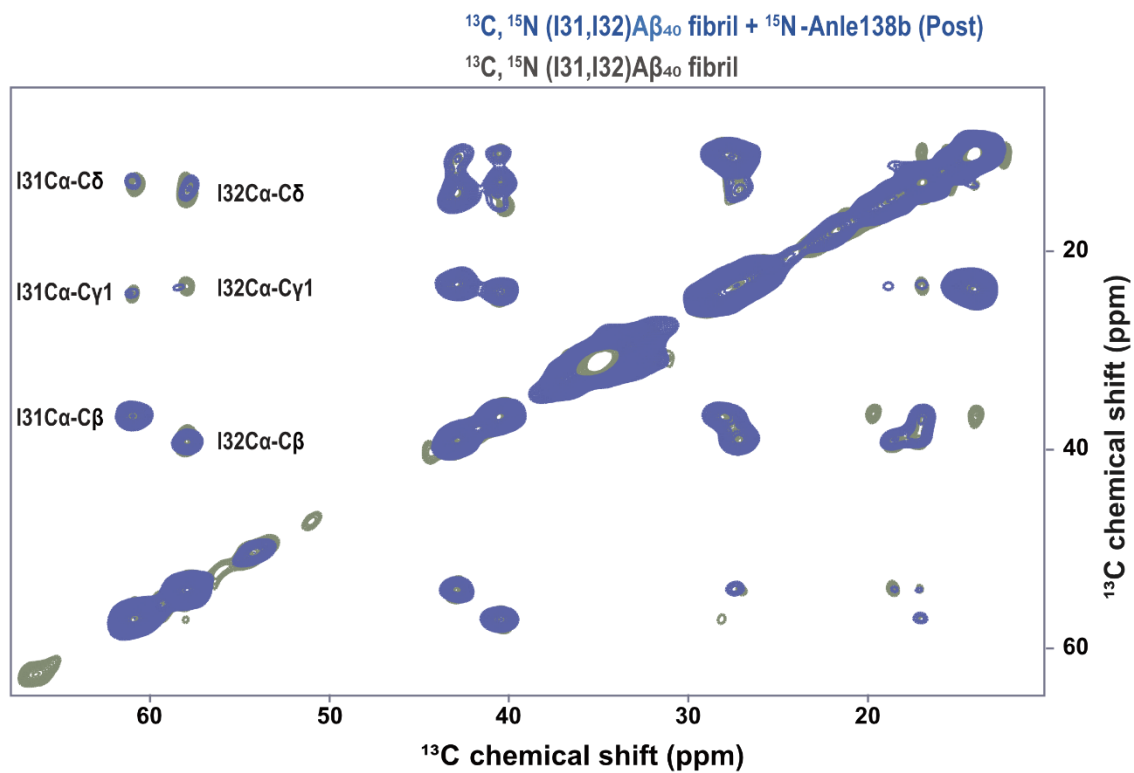
**b**



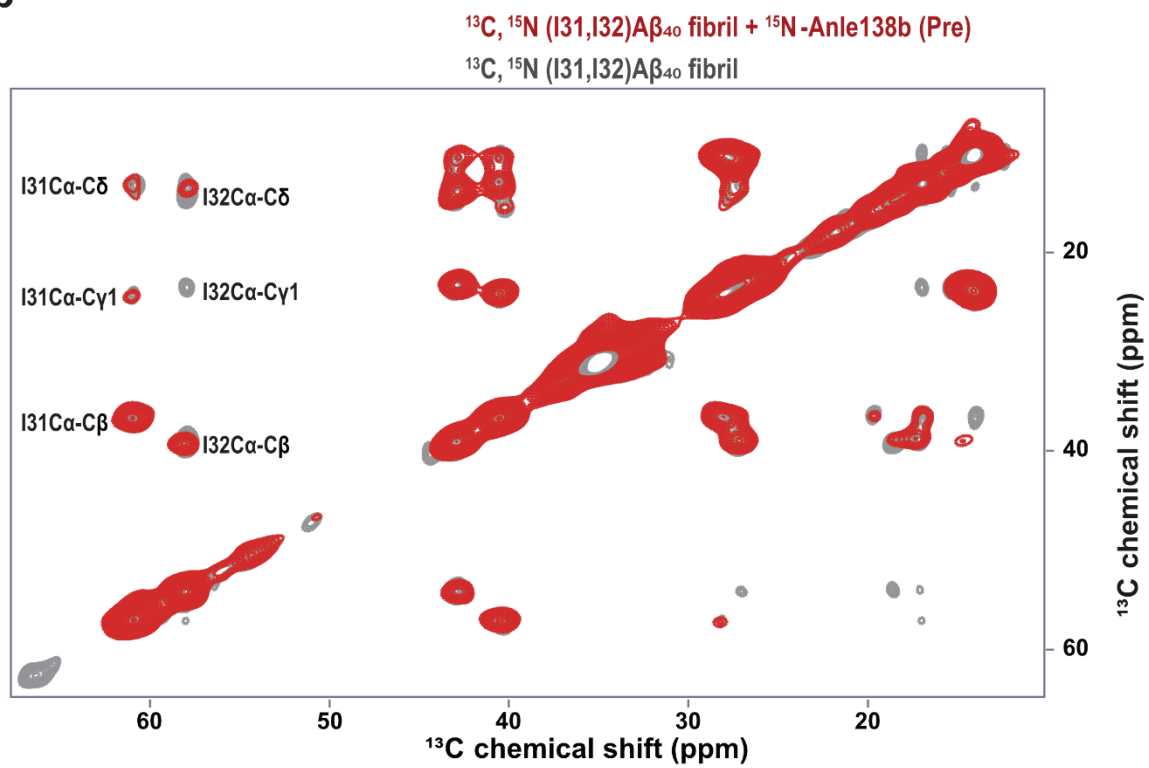
**Supplementary Figure 8 | 2D  $^{13}\text{C}$ -DARR spectra of L1 A $\beta_{40}$  fibrils selectively labeled with  $^{13}\text{C}$ ,  $^{15}\text{N}$  at Lys16 and Lys28.**

**a.** 2D  $^{13}\text{C}$ -DARR spectrum acquired at 265 K and 850 MHz with a mixing time of 20 ms. The blue spectrum corresponds to the post-treatment condition. **b.** The red spectrum represents the pre-treatment condition. In both panels, the gray spectrum represents the control condition.

**a**



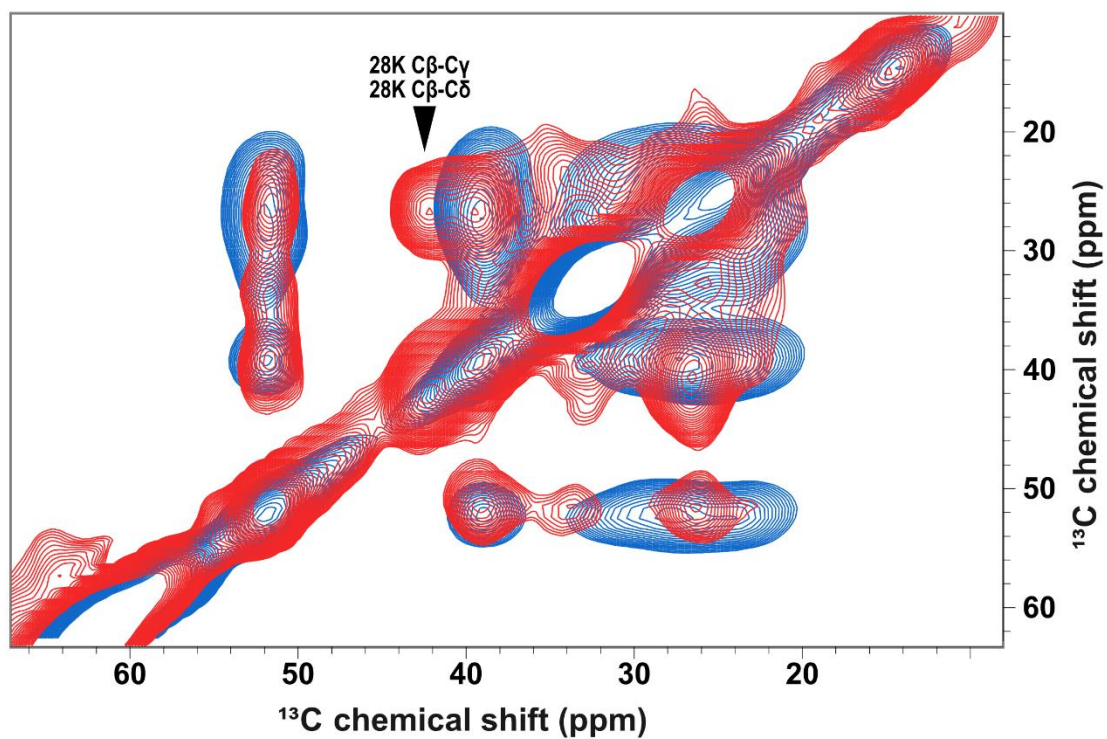
**b**



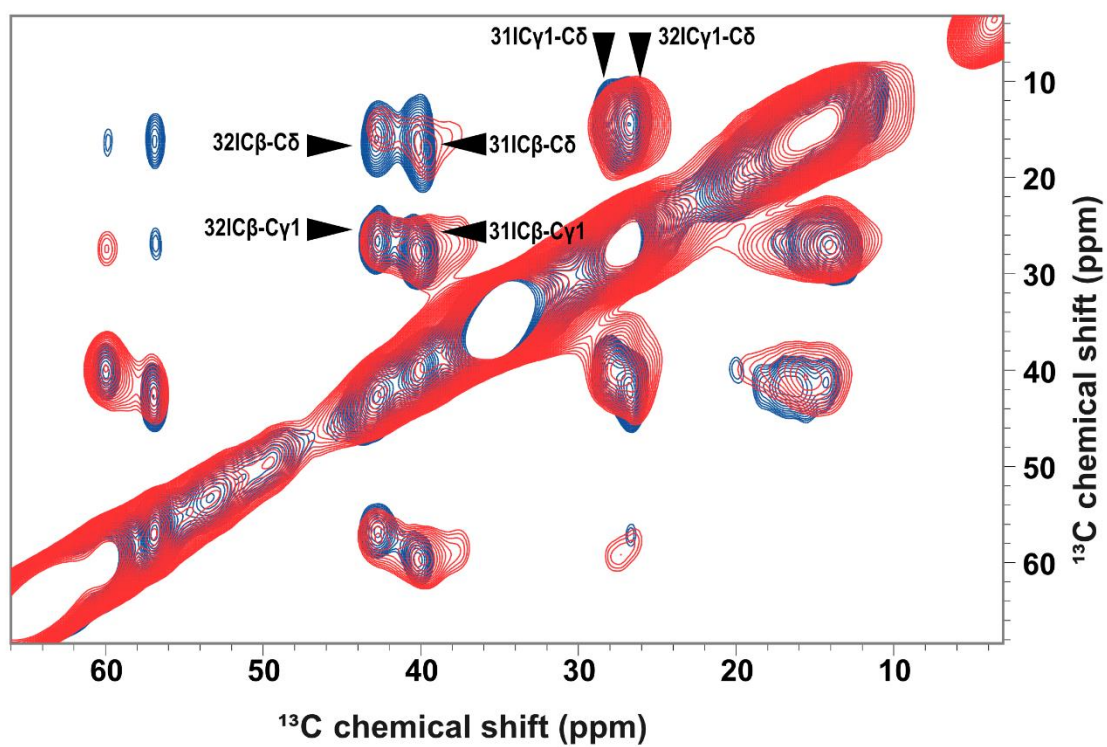
**Supplementary Figure 9 | 2D  $^{13}\text{C}^{13}\text{C}$ -DARR spectra of L1 A $\beta_{40}$  fibrils selectively labeled with  $^{13}\text{C}$ ,  $^{15}\text{N}$  at Ile31 and Ile32.**

**a.** 2D  $^{13}\text{C}^{13}\text{C}$ -DARR spectrum acquired at 265 K and 850 MHz with a mixing time of 20 ms. The blue spectrum corresponds to the post-treatment condition. **b.** The red spectrum represents the pre-treatment condition. In both panels, the gray spectrum represents the control condition.

**a**



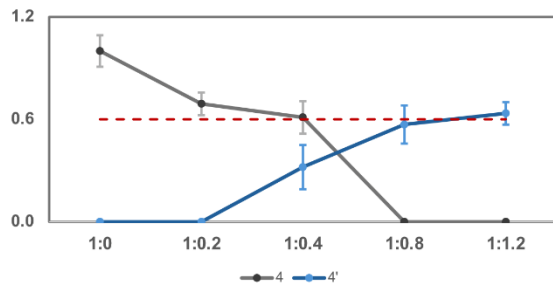
**b**



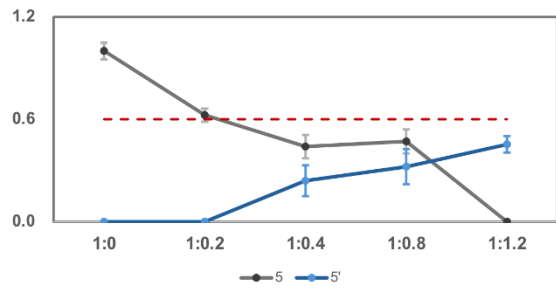
**Supplementary Figure 10 | 2D  $^{13}\text{C}^{13}\text{C}$ - DARR and RFDR spectra of selectively labeled L1 A $\beta_{40}$  fibrils used for DNP experiments.**

**a.** 2D  $^{13}\text{C}^{13}\text{C}$ -DARR spectra acquired at 100 K and 600 MHz with a mixing time of 50 ms under DNP conditions. Fibrils were selectively labeled with  $^{13}\text{C}$ ,  $^{15}\text{N}$  at Lys16 and Lys28. The blue spectrum represents the post-treatment condition, in which anle138b was added after fibril formation. The red spectrum corresponds to the pre-treatment condition, where anle138b was present during fibril formation. **b.** 2D  $^{13}\text{C}^{13}\text{C}$ -RFDR spectra acquired under the same experimental conditions, with a mixing time of 2.6 ms. Fibrils were selectively labeled with  $^{13}\text{C}$ ,  $^{15}\text{N}$  at Ile31 and Ile32. The blue spectrum corresponds to the post-treatment condition, and the red spectrum to the pre-treatment condition. Peak assignments include C $\beta$ -C $\gamma$  and C $\beta$ -C $\delta$  correlations of Lys28 (**a**), and C $\beta$ -C $\gamma$ 1 and C $\gamma$ 1-C $\delta$  correlations of Ile31 and Ile32 (**b**). Arrows indicate assigned peaks.

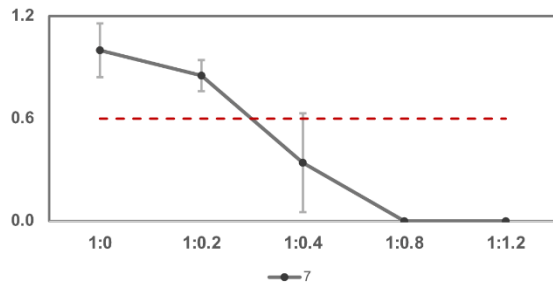
4



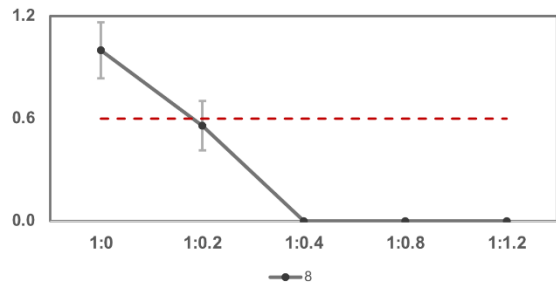
5



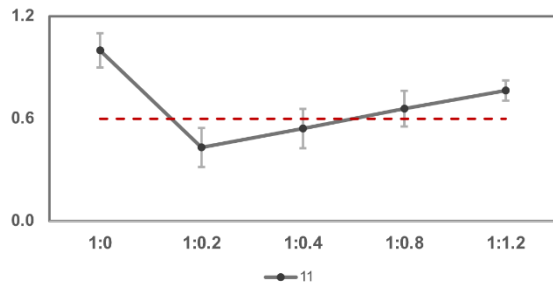
7



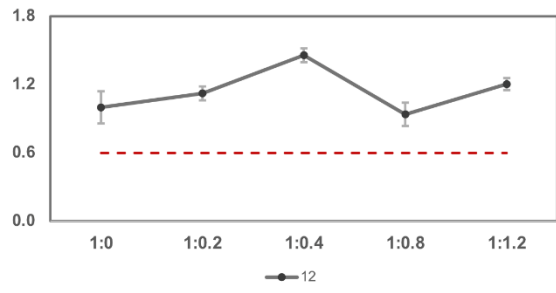
8



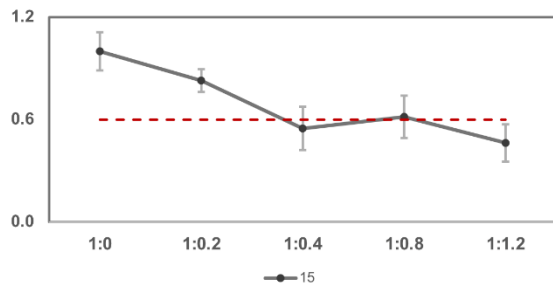
11



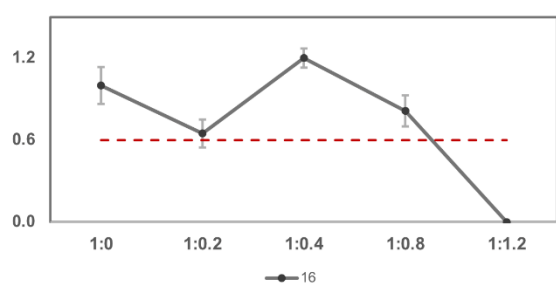
12



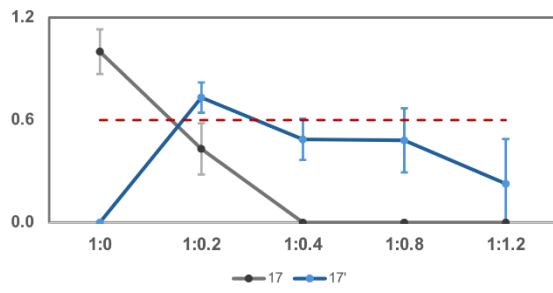
15



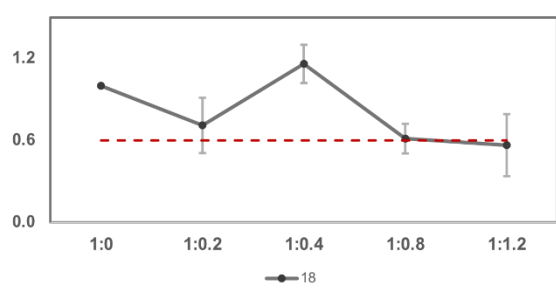
16



17



18

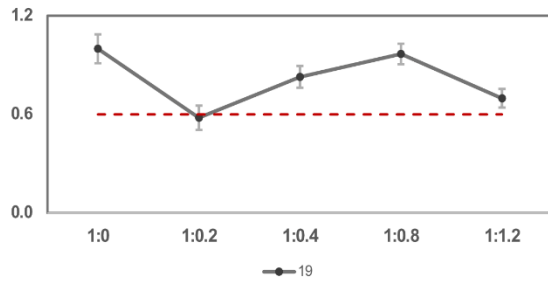


**Supplementary Figure 11 | Titration-dependent intensity changes indicating slow exchange binding of anle138b to residues 4–18 of L1 A $\beta$ <sub>40</sub> fibrils.**

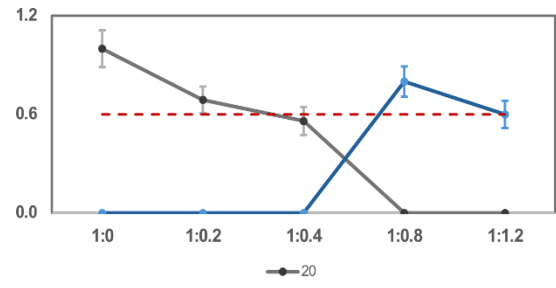
Signal intensity ratios ( $I_{\text{ratio}}$ ) were monitored for selected residues of L1 A $\beta$ <sub>40</sub> as a function of increasing anle138b molar ratios (anle138b: A $\beta$ <sub>40</sub> molar ratio (SMPR) = 0 to 1.2) under post-treatment conditions. The gray curves represent normalized intensities of original peaks ( $I_{\text{free}}$ ) observed at SMPR 0, and their changes upon ligand titration ( $I_{\text{bound}}$ ). The blue curves indicate new peaks indicative of slow exchange. The dashed red line marks the 0.6 intensity threshold used as a reference for qualitative comparison.  $I_{\text{ratio}} = I_{\text{bound}} / I_{\text{free}}$ , where  $I_{\text{free}}$  refers to the peak intensity in the absence of anle138b, and  $I_{\text{bound}}$  refers to the intensity at each titration point. Error bars indicate errors estimated from the signal-to-noise ratio of the NMR spectra. Source data are provided as a Source Data file.



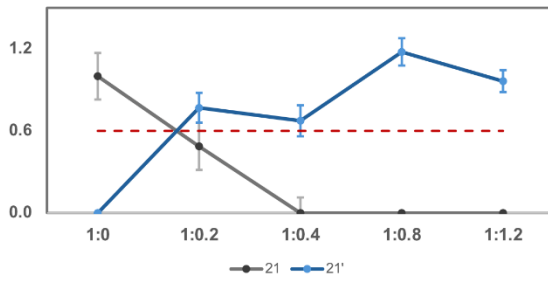
19



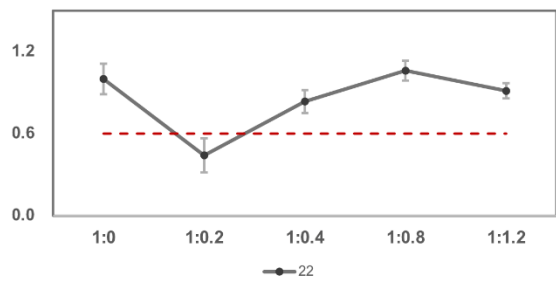
20



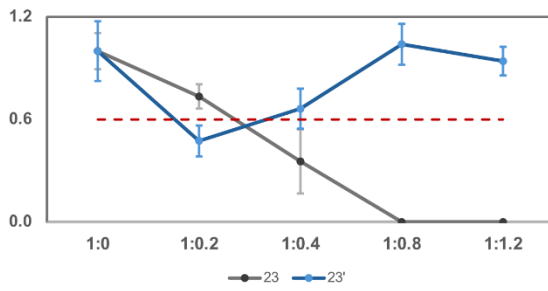
21



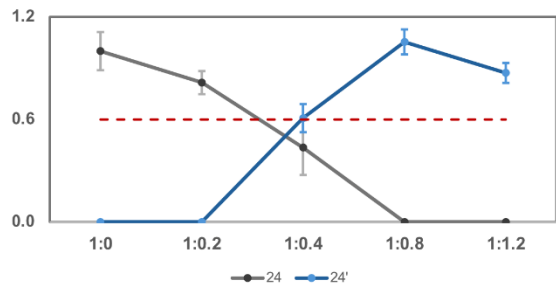
22



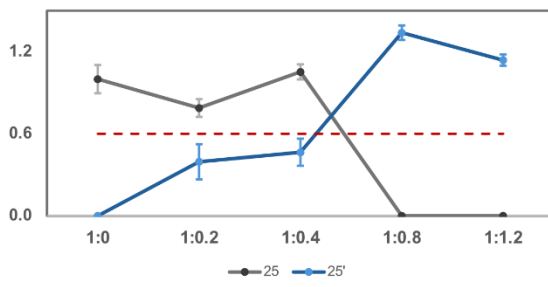
23



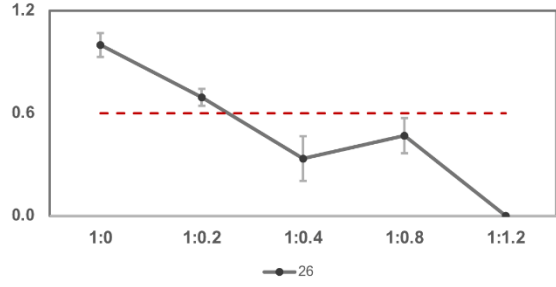
24



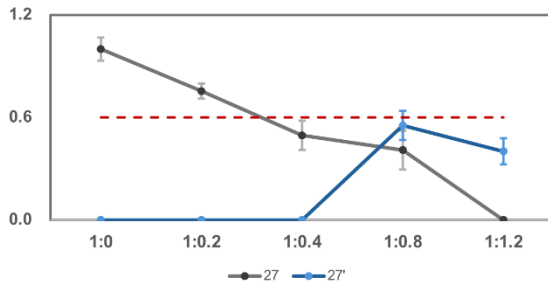
25



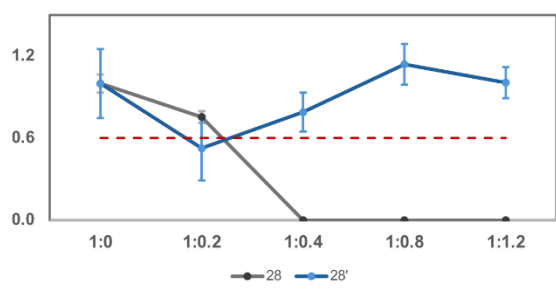
26



27

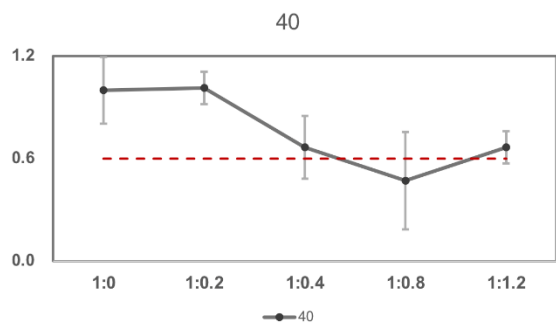
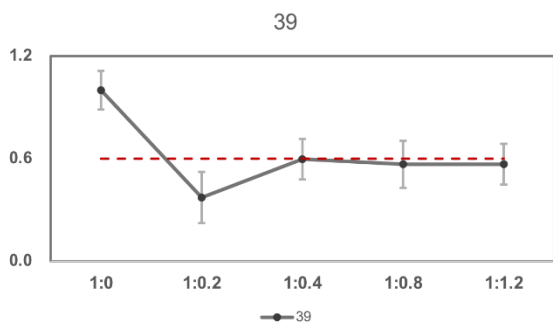
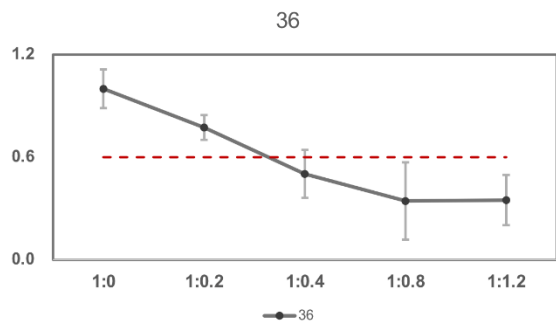
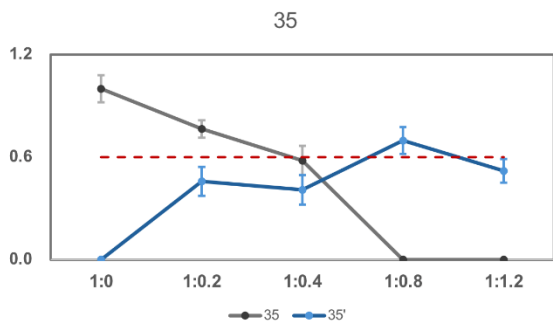
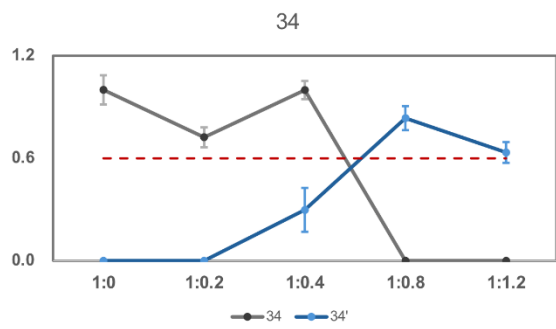
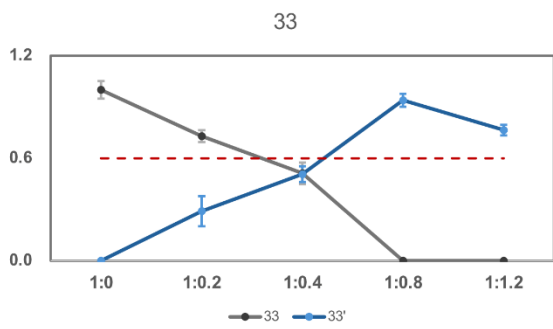
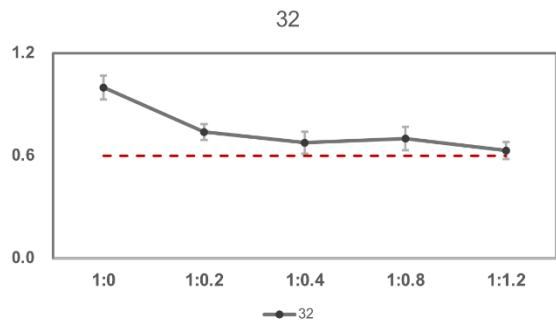
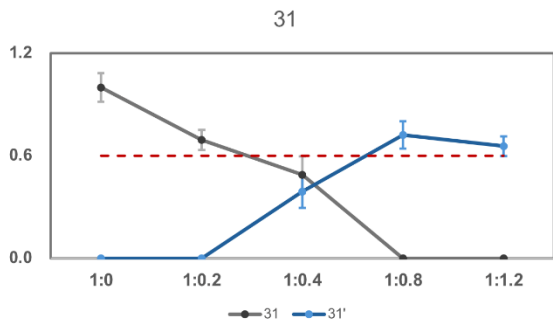
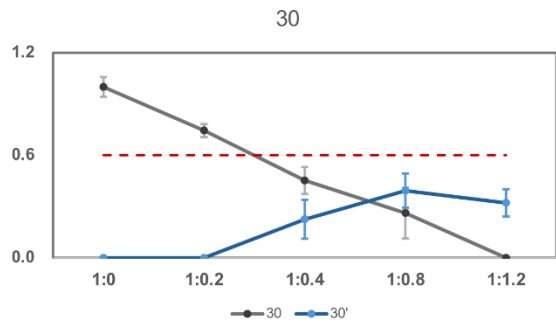
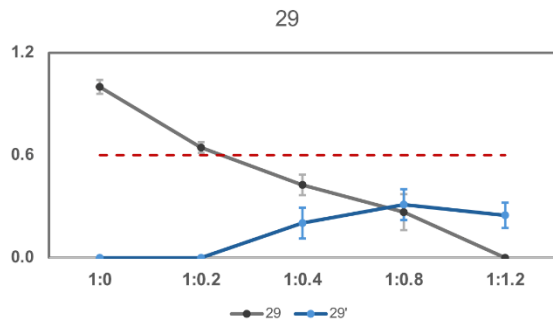


28



**Supplementary Figure 12 | Titration-dependent intensity changes indicating slow exchange binding of anle138b to residues 19–28 of L1 A $\beta$ <sub>40</sub> fibrils.**

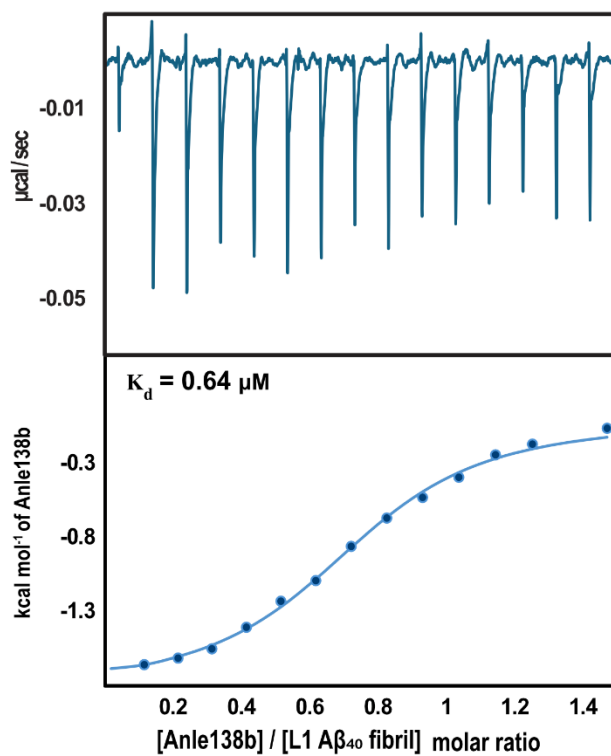
Signal intensity ratios ( $I_{\text{ratio}}$ ) were monitored for selected residues of L1 A $\beta$ <sub>40</sub> as a function of increasing anle138b molar ratios (anle138b: A $\beta$ <sub>40</sub> molar ratio (SMPR) = 0 to 1.2) under post-treatment conditions. The gray curves represent normalized intensities of original peaks ( $I_{\text{free}}$ ) observed at SMPR 0, and their changes upon ligand titration ( $I_{\text{bound}}$ ). The blue curves indicate new peaks indicative of slow exchange. The dashed red line marks the 0.6 intensity threshold used as a reference for qualitative comparison.  $I_{\text{ratio}} = I_{\text{bound}} / I_{\text{free}}$ , where  $I_{\text{free}}$  refers to the peak intensity in the absence of anle138b, and  $I_{\text{bound}}$  refers to the intensity at each titration point. Error bars indicate errors estimated from the signal-to-noise ratio of the NMR spectra. Source data are provided as a Source Data file.



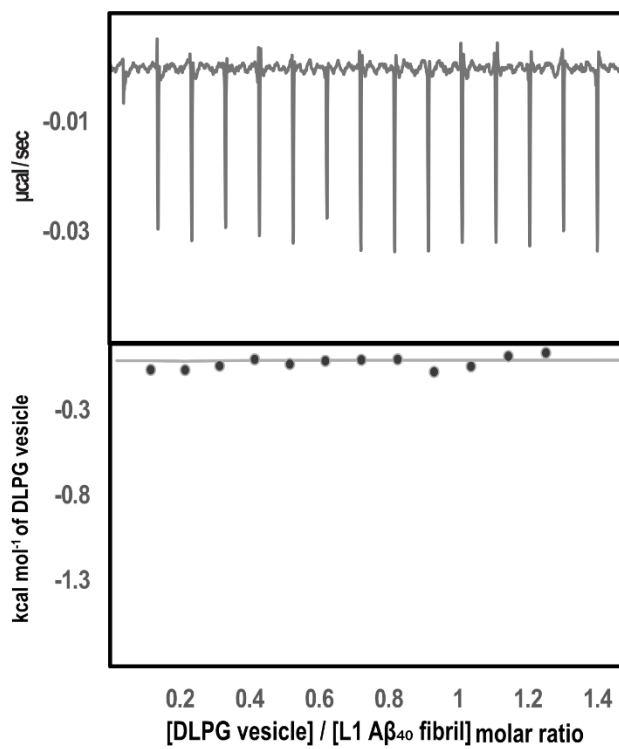
**Supplementary Figure 13 | Titration-dependent intensity changes indicating slow exchange binding of anle138b to residues 29–40 of L1 A $\beta$ <sub>40</sub> fibrils.**

Signal intensity ratios ( $I_{\text{ratio}}$ ) were monitored for selected residues of L1 A $\beta$ <sub>40</sub> as a function of increasing anle138b molar ratios (anle138b: A $\beta$ <sub>40</sub> molar ratio (SMPR) = 0 to 1.2) under post-treatment conditions. The gray curves represent normalized intensities of original peaks ( $I_{\text{free}}$ ) observed at SMPR 0, and their changes upon ligand titration ( $I_{\text{bound}}$ ). The blue curves indicate new peaks indicative of slow exchange. The dashed red line marks the 0.6 intensity threshold used as a reference for qualitative comparison.  $I_{\text{ratio}} = I_{\text{bound}} / I_{\text{free}}$ , where  $I_{\text{free}}$  refers to the peak intensity in the absence of anle138b, and  $I_{\text{bound}}$  refers to the intensity at each titration point. Error bars indicate errors estimated from the signal-to-noise ratio of the NMR spectra. Source data are provided as a Source Data file.

**a**



**b**

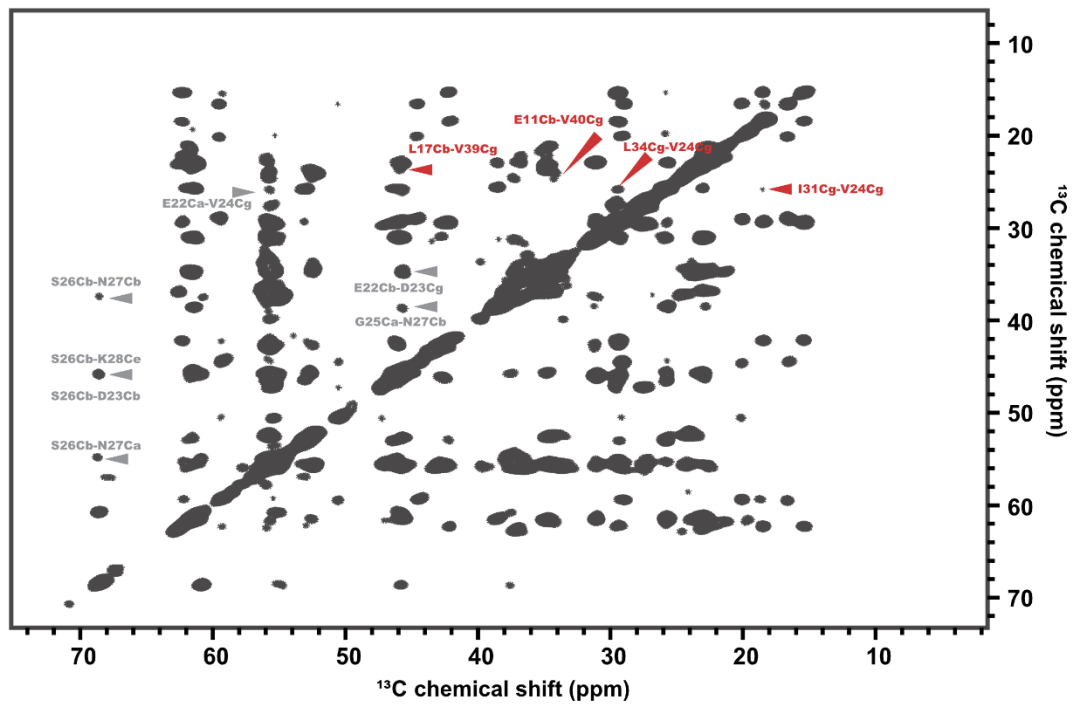


**Supplementary Figure 14 | ITC analysis of anle138b and DLPG vesicle binding to L1 A $\beta$ <sub>40</sub> fibrils.**

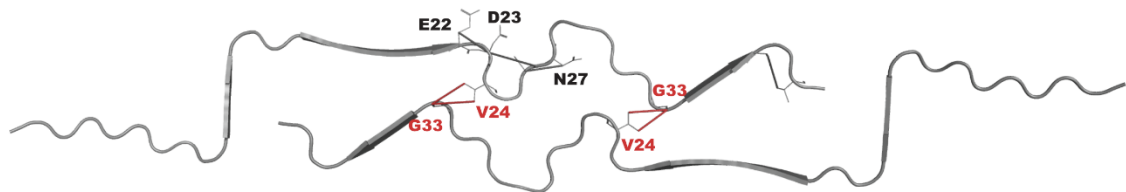
The thermodynamic parameters for binding interaction are summarized in Tab. 2.

**a.** Isothermal titration calorimetry (ITC) thermogram (top) and integrated binding isotherm (bottom) of anle138b (100  $\mu$ M), formulated in DLPG vesicles (2 mM), titrated into L1 A $\beta$ <sub>40</sub> fibrils (10  $\mu$ M). The fitted curve yields a dissociation constant ( $K_d$ ) of 0.64  $\mu$ M and a binding stoichiometry of ~0.72 anle138b molecules per A $\beta$ <sub>40</sub> monomer. **b.** Negative control: Titration of DLPG vesicles (2 mM) into L1 A $\beta$ <sub>40</sub> fibrils (10  $\mu$ M) produces negligible heat and a flat isotherm, indicating no detectable interaction between vesicles and fibrils. Source data are provided as a Source Data file.

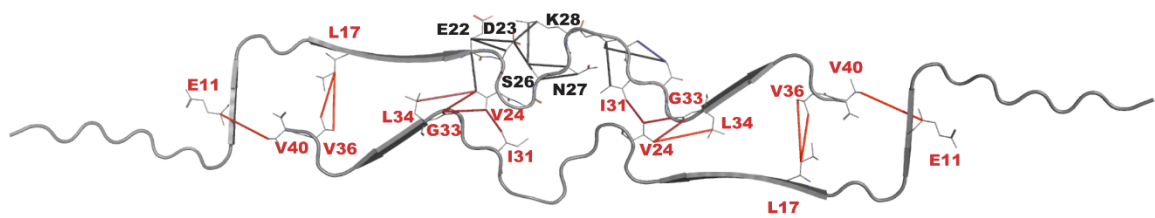
**a**



**b**



**c**

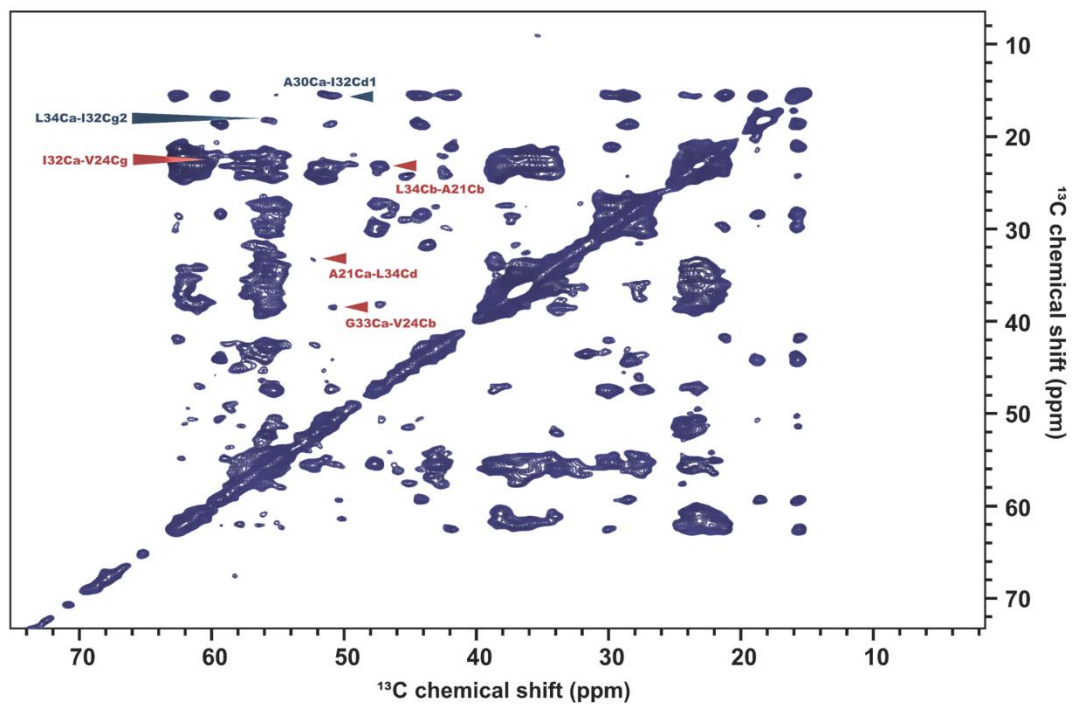


**Supplementary Figure 15 | 2D  $^{13}\text{C}$ - $^{13}\text{C}$ -DARR spectrum (265K, 850MHz) of L1 A $\beta_{40}$  fibrils.**

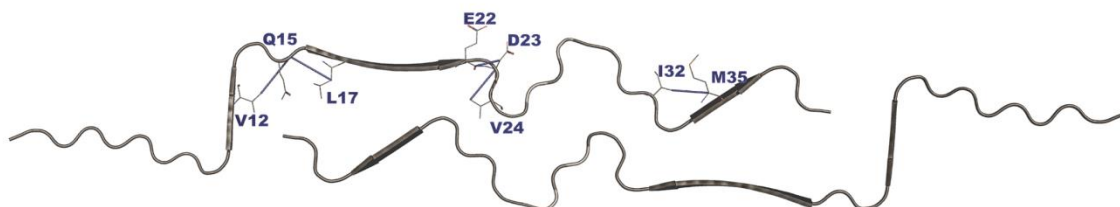
**a.** Aliphatic region of the 2D  $^{13}\text{C}$ - $^{13}\text{C}$  chemical shift correlation spectrum acquired at 265 K and 850 MHz (mixing time = 200 ms). Gray arrows indicate medium-range intramolecular cross-peaks (2–4 Å); red arrows indicate medium-to-long-range intermolecular cross-peaks (3–5 Å). **b.** The structural model of L1 A $\beta_{40}$  fibrils shows the intramolecular contacts (gray bars, mixing time = 50 ms). **c.** The same structural model highlights the intra- and intermolecular contacts (gray and red bars, respectively, mixing time = 200 ms).



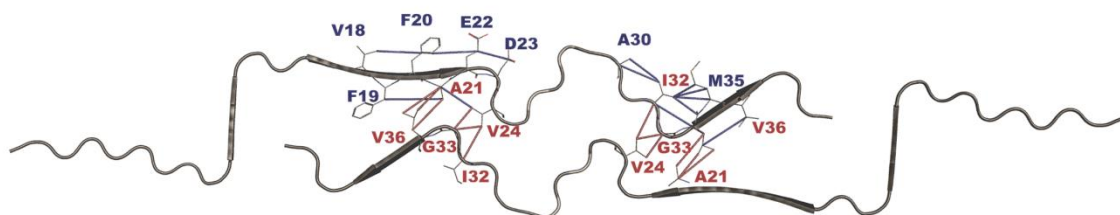
**a**



**b**

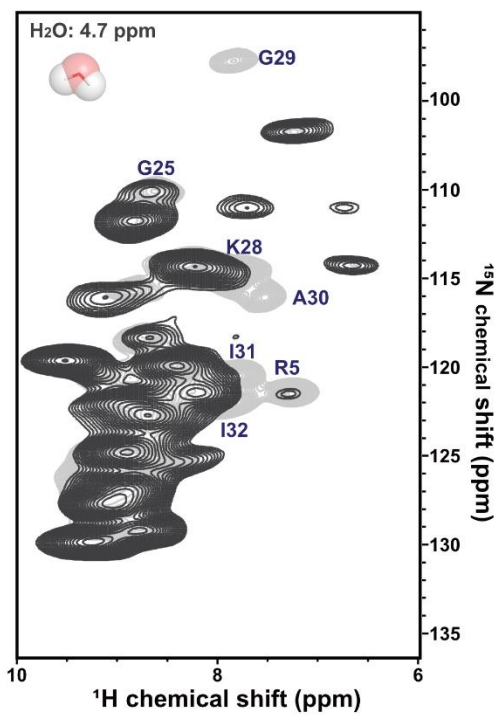
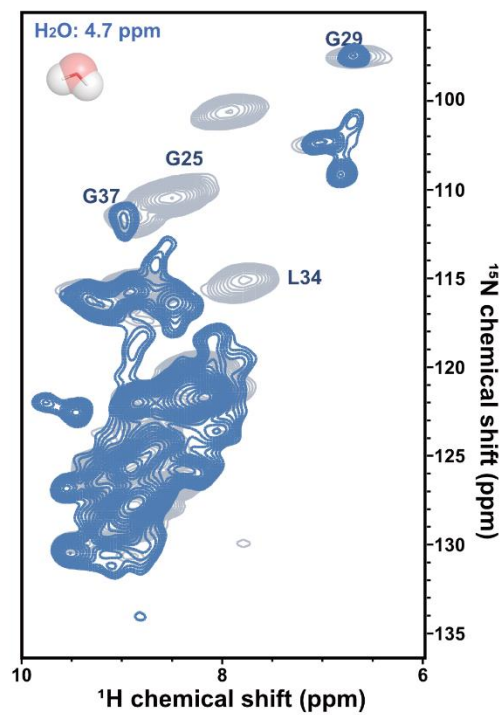
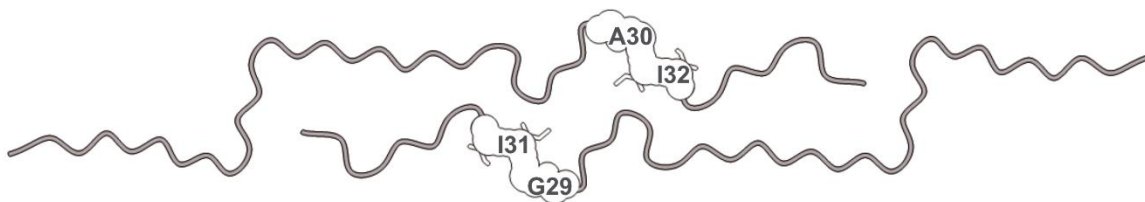


**c**



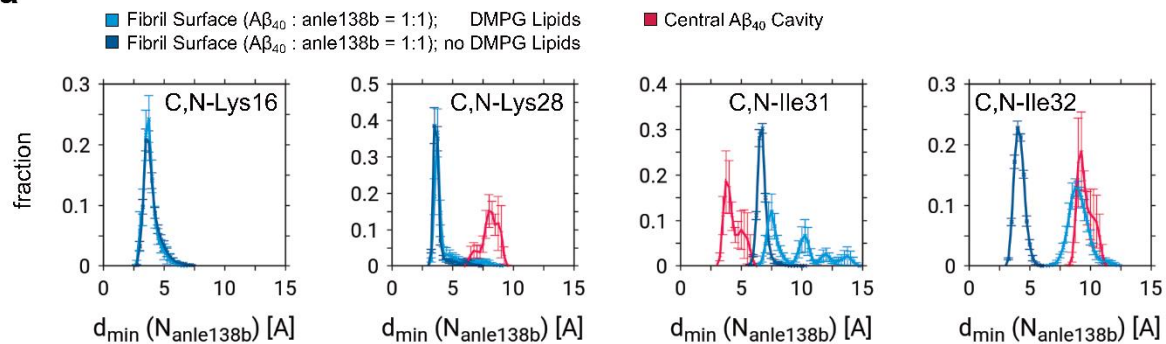
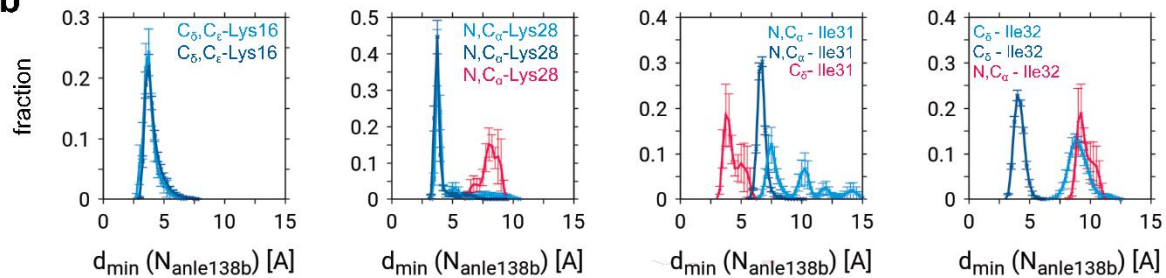
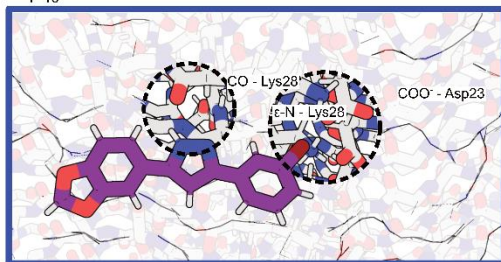
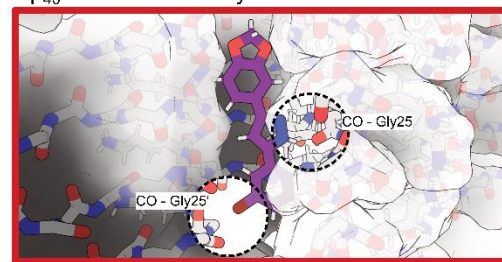
**Supplementary Figure 16 | 2D  $^{13}\text{C}$ - $^{13}\text{C}$ -DARR spectrum (265K, 850MHz) of L1 A $\beta_{40}$  fibrils (post-treatment condition).**

Anle138b was applied to L1 A $\beta_{40}$  fibrils after fibril formation (anle138b: A $\beta_{40}$  molar ratio (SMPR) = 1.2). **a.** Aliphatic region of the 2D  $^{13}\text{C}$ - $^{13}\text{C}$  chemical shift correlation spectrum acquired at 265 K and 850 MHz (mixing time = 200 ms). Blue arrows indicate medium-range intramolecular cross-peaks (2–4 Å); red arrows indicate medium-to-long-range intermolecular cross-peaks (3–5 Å). **b.** The structural model of L1 A $\beta_{40}$  fibrils shows the intramolecular contacts (blue bars, mixing time = 50 ms). **c.** The same structural model highlights the intra- and intermolecular contacts (blue and red bars, respectively, mixing time = 200 ms).

**a****b****c****d**

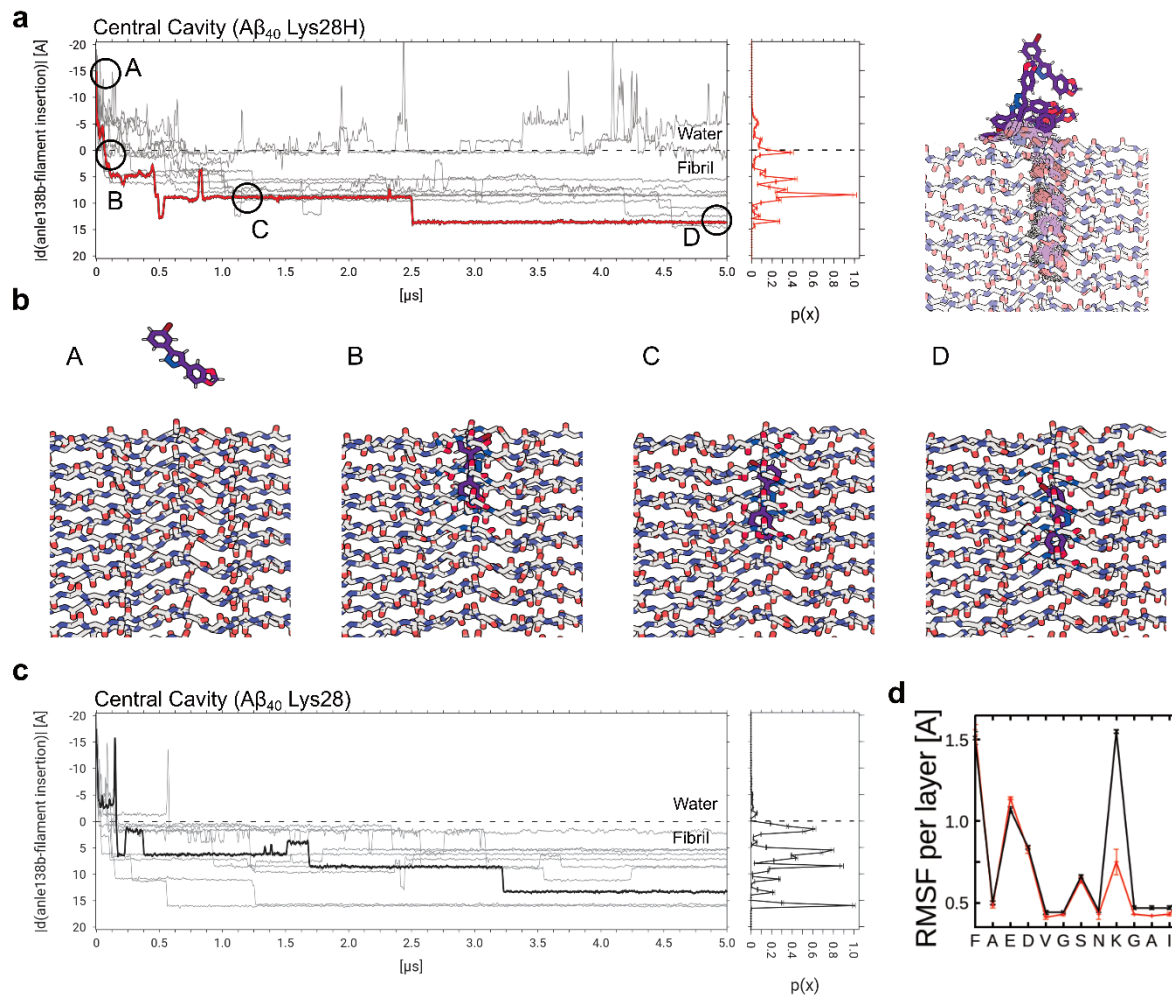
**Supplementary Figure 17 | Comparison of H<sub>2</sub>O-accessible amide groups in L1 A $\beta$ <sub>40</sub> fibrils under control and post-treatment conditions.**

**a.** Light gray: 2D (H)NH spectrum of <sup>2</sup>H, <sup>13</sup>C, <sup>15</sup>N-labeled L1 A $\beta$ <sub>40</sub> fibrils (control). Dark gray: 2D plane at 4.7 ppm (water signal) in the H dimension was extracted from a 3D H(H)NH NOE spectrum with a 50 ms mixing time. Cross-peaks in dark gray indicate amide groups in close contact with H<sub>2</sub>O under control conditions. **b.** Light gray: 2D (H)NH spectrum of <sup>2</sup>H, <sup>13</sup>C, <sup>15</sup>N-labeled L1 A $\beta$ <sub>40</sub> fibrils under post-treatment conditions. Blue: 2D slice from a 3D H(H)NH NOE spectrum (50 ms mixing) at 4.7 ppm. Blue cross-peaks indicate water-accessible amides in the post-treatment condition. **c.** Structural map of control fibrils, with gray-colored residues indicating H<sub>2</sub>O-accessible amides. **d.** Structural map of post-treatment fibrils, with blue-colored residues indicating water-accessible amides. Residues with no detectable water contact are shown as white spheres.

**a****b****c** $A\beta_{40}$  L1 Fibril Surface $A\beta_{40}$  L1 Central Cavity

**Supplementary Figure 18 | Dominant binding poses and interatomic contacts of surface-bound and internally bound anle138b.**

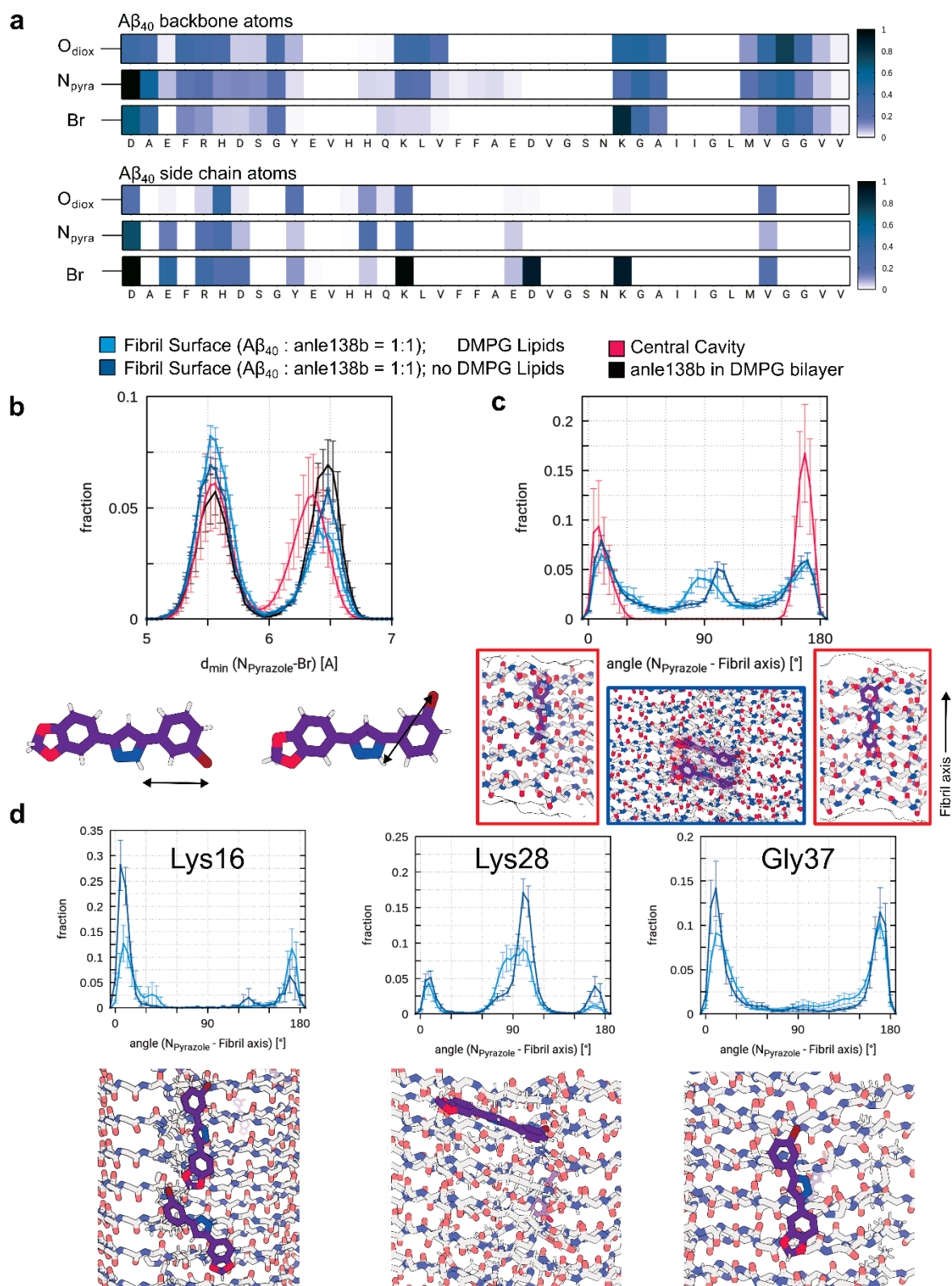
**a.** Distributions of minimum distances derived from all N or C atoms of residues K16, K28, I31, and I32 to anle138b pyrazole nitrogen atoms for the simulation sets representing either surface-bound (blue and dark blue: without DMPG) or internally bound (red) anle138b. **b.** Distributions of minimum distances derived from the individual N and/or C atoms of residues K16, K28, I31, and I32 to anle138b pyrazole nitrogen atoms that best fit the distributions in **a** and **c**. For panels **a** and **b**, data are presented as mean  $\pm$  SEM (indicated by error bars) for 10 replicates, respectively. Representative MD simulation snapshot of anle138b binding poses and interatomic contacts as observed for L1 A $\beta$ <sub>40</sub> surface-bound (left panel) or internally bound (right panel). Circles highlight interatomic contacts: Lys28 carbonyl to anle138b pyrazole and Asp23/Lys28 side chain to anle138b bromophenyl interaction (left), as well as Gly25 carbonyl to anle138b pyrazole and Gly25 carbonyl (opposing protofilament) to anle138b bromophenyl interaction (right). DMPG lipids are not shown for clarity.



**Supplementary Figure 19 | Anle138b inserts spontaneously in the central cavity of A $\beta$ <sub>40</sub> L1 fibrils.**

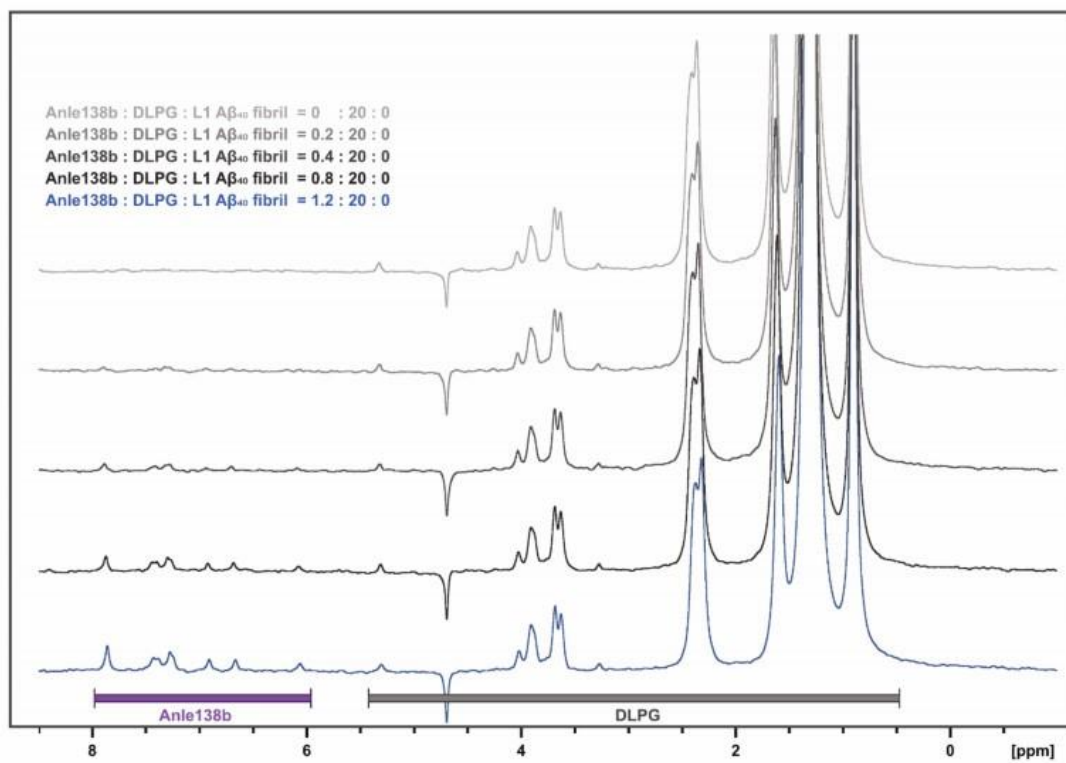
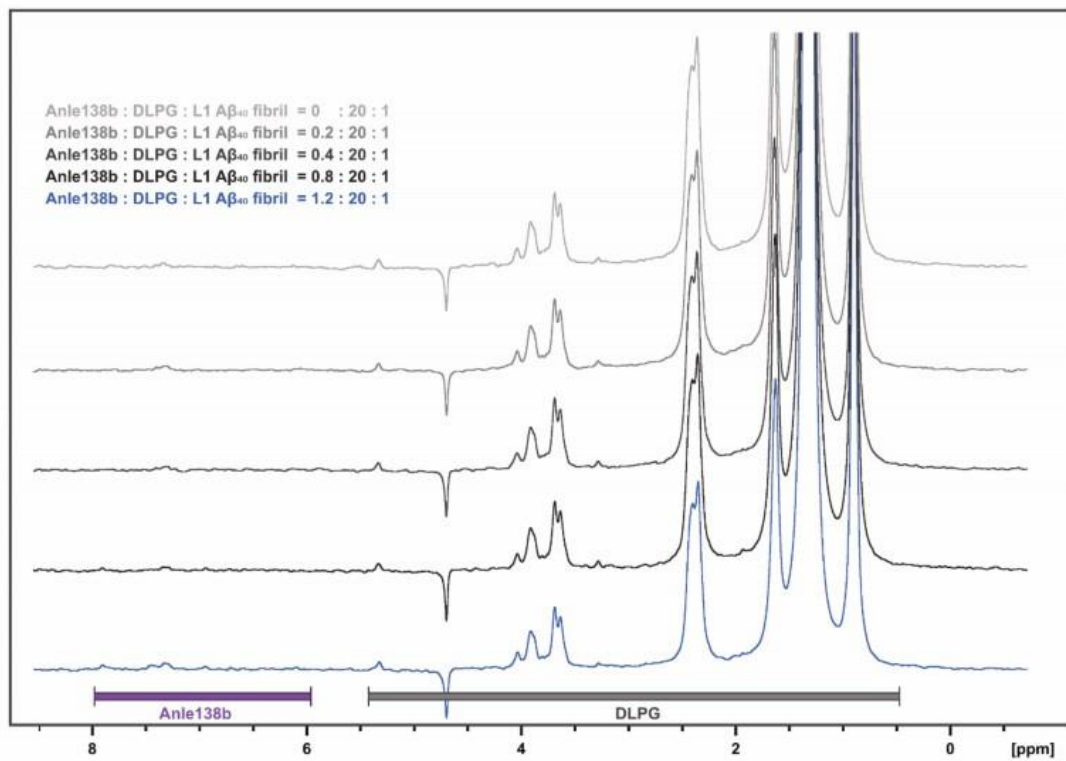
**a.** Distance of the anle138b pyrazole nitrogen atoms to the fibril center-of-mass (representative trajectory as bold lines: color red; others as shaded thin lines for clarity: color gray) and **b.** snapshots (A, B, C, D) from MD simulations of anle138b spontaneously binding internally to the cavity of L1, as well as its discrete translational motion along the fibril axis. **c.** Distance of the anle138b pyrazole nitrogen atoms to the fibril center-of-mass for simulations with deprotonated Lys28 i.e. disrupted hydrogen bond interaction between Asp23 and Lys28. The **histograms** (panels on the right) in **a** and **c** were calculated over the full trajectory length, respectively. Simulations in **a** show that deeper or comparable insertion to **c** does not occur on the multi  $\mu$ s-time scales accessible by the reported MD simulations. **d.** Average root mean squared fluctuations (RMSF) for residues of the loop region with (red) and without (black) intact Asp23-Lys28 hydrogen bond. Data are presented as mean values  $\pm$  SEM (depicted by error bars). Source data are provided as a Source Data file.





**Supplementary Figure 20 | Anle138b binding modes to the surface and central cavity of L1 A $\beta$ <sub>40</sub> fibrils.**

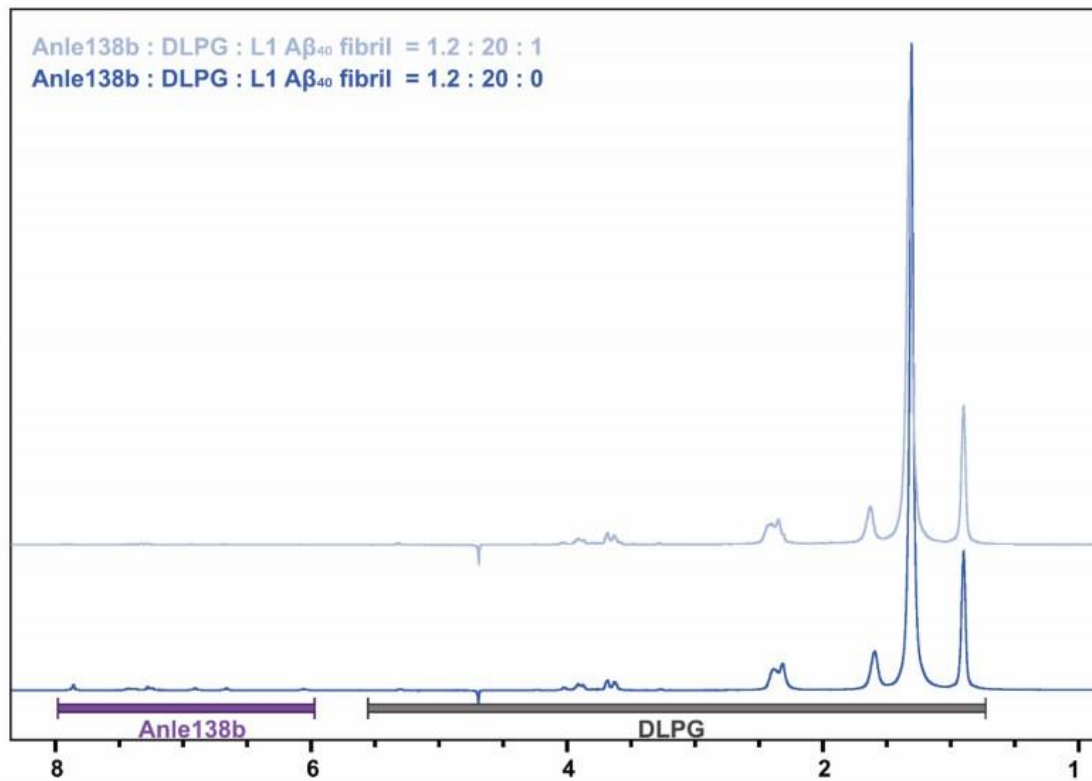
**a.** Heat maps report polar contacts between backbone and side chain atoms of individual L1 A $\beta$ <sub>40</sub> fibril structure residues and polar moieties of anle138b, respectively. Scale bars indicate contact probabilities. **b.** Distance distribution of anle138b pyrazole N to Bromine atom (blue – surface-bound anle138b; red - internal binding pose, black – anle138b in DMPG bilayer). Data are presented as mean  $\pm$  s.e.m. (indicated by error bars) for 10 replicates, respectively. **c.** Anle138b alignment with respect to the fibril axis when bound either internally to the loop region (red) or to the surface of the L1 A $\beta$ <sub>40</sub> fibrils (blue). Data are presented as mean  $\pm$  s.e.m. (indicated by error bars) for 10 replicates, respectively. **d.** Anle138b alignment with respect to the fibril axis when bound to residues Lys16, Lys28, and Gly37 of the L1 A $\beta$ <sub>40</sub> fibril surface. Data are presented as mean  $\pm$  s.e.m. (indicated by error bars) for 10 replicates, respectively. Representative snapshots of anle138b binding poses are shown. DMPG lipids are not depicted for clarity. Source data are provided as a Source Data file.

**a****b**

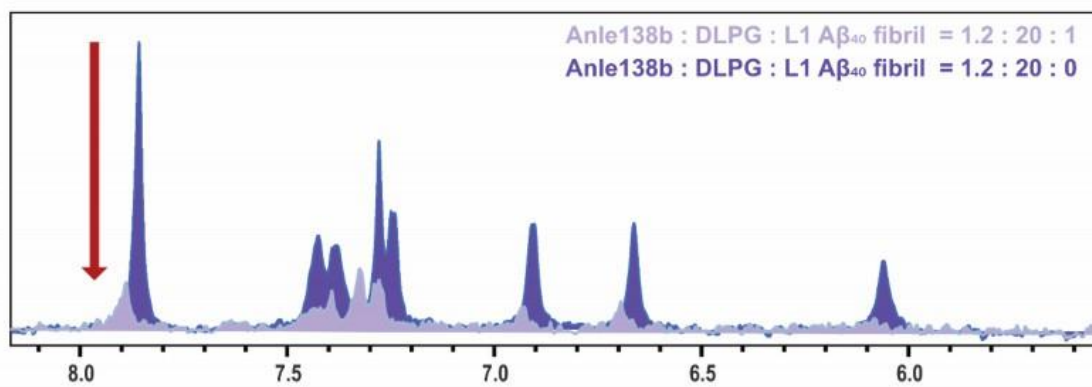
**Supplementary Figure 21 | 1D  $^1\text{H}$  NMR spectra showing anle138b incorporation into DLPG vesicles and its binding to L1  $\text{A}\beta_{40}$  fibrils under post-treatment conditions.**

**a.** 1D  $^1\text{H}$  NMR spectra (ns=128) showing increasing concentrations of anle138b incorporated into DLPG vesicles. The purple region indicates anle138b signals, and the gray region indicates DLPG signals. **b.** 1D  $^1\text{H}$  NMR spectra (ns=128) of the supernatant obtained after ultracentrifugation of L1  $\text{A}\beta_{40}$  fibrils treated under the conditions shown in panel a (after 1h 37°C. incubation). The decrease in free anle138b signals with increasing concentration indicates that most anle138b is bound to the fibrils.

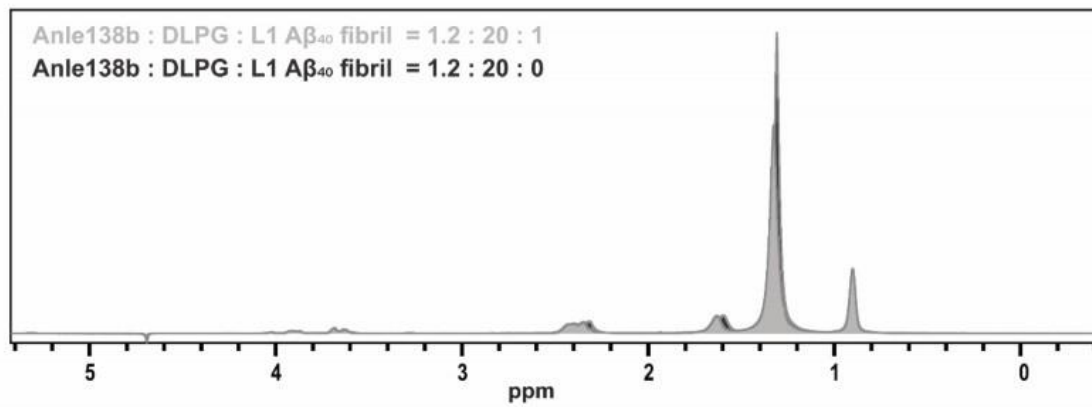
**a**



**b**

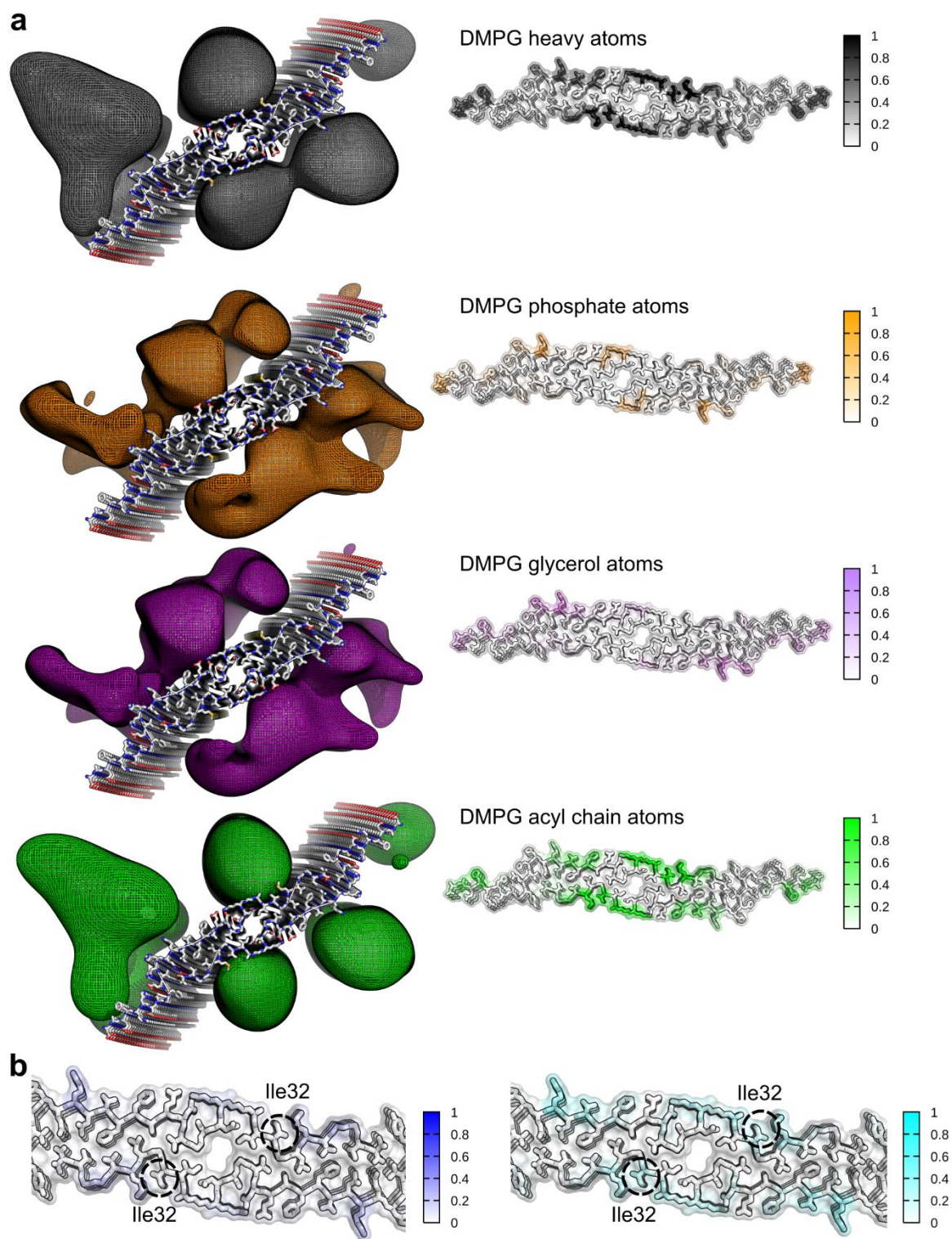


**c**



**Supplementary Figure 22 |  $^1\text{H}$  NMR spectra showing the decrease of free anle138b in the supernatant after incubation with L1  $\text{A}\beta_{40}$  fibrils.**

**a.** Overlaid  $^1\text{H}$  NMR spectra (ns=1024) of samples without  $\text{A}\beta_{40}$  fibrils (dark blue) and with fibrils (light blue). The fibril-containing sample was incubated with anle138b and  $\text{A}\beta_{40}$  fibrils at a 1.2:1 molar ratio for 1 hour, followed by ultracentrifugation, and only the supernatant was analyzed. **b.** In the  $\delta$  8.0–6.0 ppm region, the anle138b peaks highlighted in purple showed a significant decrease after fibril treatment (red arrow). **c.** In the  $\delta$  5.0–0.5 ppm region, the DLPG peaks highlighted in gray remained nearly unchanged under both conditions, indicating a consistent amount of vesicles and serving as a reference for quantification. Quantitative analysis revealed approximately a 70% decrease in the integrated anle138b peak, with the signal-to-noise ratio (S/N) dropping from 52.1 to 11.0. This suggests that a substantial amount of anle138b was bound to or removed by the fibrils, resulting in its depletion from the supernatant.

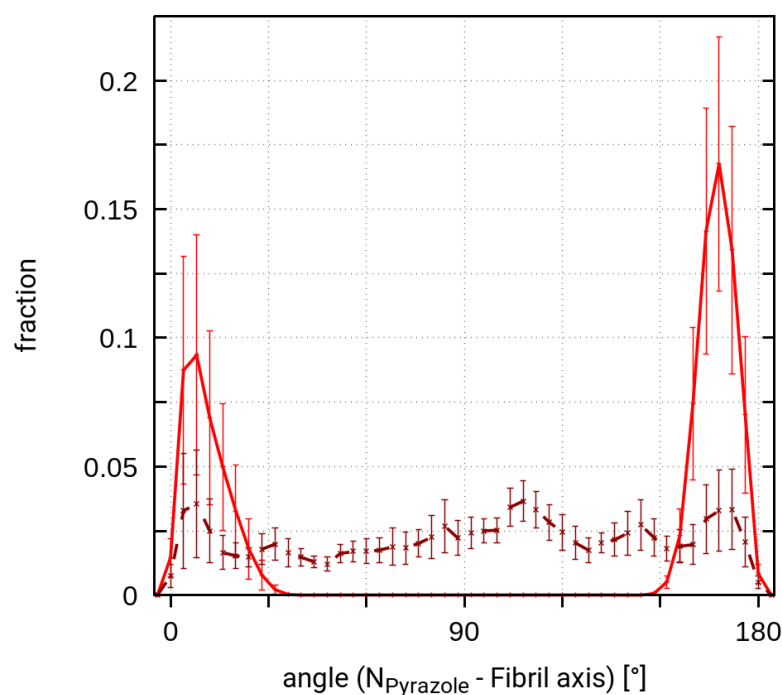


**Supplementary Figure 23 | Determination of the binding region on L1 A $\beta$ <sub>40</sub> fibrils for lipids.**

(a, left) 3D probability density of the DMPG lipid atomic positions and (a, right) atomic models with residues colored according to their interaction frequencies with all lipid heavy atoms

(black), the phosphate group (orange), glycerol group (purple), the acyl chains (green) throughout the MD simulations for the L1 A $\beta$ <sub>40</sub> fibril structure. Density maps were visualized as isomesh and contoured at 2 $\sigma$ . **(b)** Interaction frequencies of anle138b nitrogen atoms with residues of the L1 A $\beta$ <sub>40</sub> fibril structure (left – in the presence of DMPG, right – in the absence of DMPG). The location of residue I32 is highlighted by a black circle. Residues are colored with the color saturation linearly increasing with interaction frequencies between 0 and 100%. Source data are provided as a Source Data file.





**Supplementary Figure 24 | Anle138b orientations in MD simulations of truncated fibril models with flat-bottomed potentials around the central cavity of L1 A $\beta$ <sub>40</sub> fibrils.**

Anle138b alignment with respect to the fibril axis and when bound either internally to the central loop region (red solid line, as shown in Fig. S19) or unbound during the MD simulations of truncated fibril models (dark-red broken line). Data are presented as mean  $\pm$  s.e.m. (indicated by error bars). Source data are provided as a Source Data file.

**Supplementary Table 1 | Experimental parameters of NMR data acquisition on the sample.**

Exp	Spectrometer	MAS (kHz) rotor	Transfer	Nucleus	time cp (ms)	rf (kHz)	Ramp	Temperature	Sample
3D (H)CANH	800, Advance III	55 (1.3mm)	$^1\text{H}$ - $^{13}\text{C}$ -CP	$^1\text{H}$	6.5	96	80-100%	235K	$^2\text{H}$ , $^{13}\text{C}$ , $^{15}\text{N}$ A $\beta_{40}$ fibril  $^2\text{H}$ , $^{13}\text{C}$ , $^{15}\text{N}$ A $\beta_{40}$ fibril: Anle138b = 1:0.2, 1: 0.4, 1:0.8, 1:1.2 (titration)
				$^{13}\text{C}$		88	square		
			$^{13}\text{C}$ - $^{15}\text{N}$ -CP	$^{13}\text{C}$	20	139.1	tangent		
				$^{15}\text{N}$		57	square		
			$^{15}\text{N}$ - $^1\text{H}$ -CP	$^1\text{H}$		145	100-80%		
				$^{15}\text{N}$	0.7	85			
3D (H)coCAcoNH	800, Advance III	55 (1.3mm)	$^1\text{H}$ - $^{13}\text{C}$ -CP	$^1\text{H}$	2.9	22	85-100%	235K	$^2\text{H}$ , $^{13}\text{C}$ , $^{15}\text{N}$ A $\beta_{40}$ fibril: Anle138b = 1:1.2
				$^{13}\text{C}$		17	square		
			$^{13}\text{C}$ - $^{15}\text{N}$ -CP	$^{13}\text{C}$	25	17	tangent		
				$^{15}\text{N}$		15	square		
			$^{15}\text{N}$ - $^1\text{H}$ -CP	$^1\text{H}$	8	24	100-80%		
				$^{15}\text{N}$	0.85	20.7			
2D (H)NH	800, Advance III	55 (1.3mm)	$^{15}\text{N}$ - $^1\text{H}$ -CP	$^1\text{H}$	3.1	97	100-80%	235K	$^2\text{H}$ , $^{13}\text{C}$ , $^{15}\text{N}$ A $\beta_{40}$ fibril: Anle138b = 1:1.2
				$^{15}\text{N}$		170			
			$^1\text{H}$ - $^{15}\text{N}$ -CP	$^1\text{H}$	0.9	104	80-100%		
				$^{15}\text{N}$		170			
3D H(H)NH NOE	800, Advance III	55 (1.3mm)	$^{15}\text{N}$ - $^1\text{H}$ -CP	$^1\text{H}$	3.1	90	100-80%	235K	$^2\text{H}$ , $^{13}\text{C}$ , $^{15}\text{N}$ A $\beta_{40}$ fibril: Anle138b = 1:1.2
				$^{15}\text{N}$		152			
			$^1\text{H}$ - $^{15}\text{N}$ -CP	$^1\text{H}$	0.9	99	80-100%		

				$^{15}\text{N}$		166			
2D $^{13}\text{C}$ - $^{13}\text{C}$ -DARR (20ms, 50ms, 200ms, 400ms)	850, NEO	17 (3.2mm)	$^1\text{H}$ - $^{13}\text{C}$ -CP	$^1\text{H}$		80	100-80%	265K	$^1\text{H}$ , $^{13}\text{C}$ , $^{15}\text{N}$ A $\beta_{40}$ fibril  $^1\text{H}$ , $^{13}\text{C}$ , $^{15}\text{N}$ A $\beta_{40}$ fibril: Anle138b = 1:1.2 (Post-treatment condition)  $^1\text{H}$ , $^{13}\text{C}$ , $^{15}\text{N}$ A $\beta_{40}$ fibril: Anle138b = 1:1.2 (Pre-treatment condition)
				$^{13}\text{C}$	1.1	88			
3D (H)CANH	850, NEO	55 (1.3mm)	$^1\text{H}$ - $^{13}\text{C}$ -CP	$^1\text{H}$	2.9	22	85-100%	235K	$^1\text{H}$ , $^{13}\text{C}$ , $^{15}\text{N}$ A $\beta_{40}$ fibril
				$^{13}\text{C}$		17	square		
			$^{13}\text{C}$ - $^{15}\text{N}$ -CP	$^{13}\text{C}$	25	17	tangent		
				$^{15}\text{N}$		15	square		
			$^{15}\text{N}$ - $^1\text{H}$ -CP	$^1\text{H}$		24	100-80%		
				$^{15}\text{N}$	0.8	20.7			
2D (H)NCA	850, NEO	17 (3.2mm)	$^{13}\text{C}$ - $^{15}\text{N}$ -CP	$^{13}\text{C}$	3	16	100-90%	265K	$^1\text{H}$ , $^{13}\text{C}$ , $^{15}\text{N}$ A $\beta_{40}$ fibril  $^1\text{H}$ , $^{13}\text{C}$ , $^{15}\text{N}$ A $\beta_{40}$ fibril: Anle138b = 1:1.2 (Pre-treatment condition)  $^1\text{H}$ , $^{13}\text{C}$ , $^{15}\text{N}$ A $\beta_{40}$ fibril: Anle138b = 1:1.2 (Pre-treatment condition)
				$^{15}\text{N}$		18			
			$^1\text{H}$ - $^{15}\text{N}$ -CP	$^1\text{H}$	1.5	83	80-100%		
				$^{15}\text{N}$		73			

2D $^{13}\text{C}$ - $^{13}\text{C}$ -DARR (20ms)	850, NEO	17 (3.2mm)	$^1\text{H}$ - $^{13}\text{C}$ -CP	$^1\text{H}$		80	100-80%	265K	ILE $^{13}\text{C}$ , $^{15}\text{N}$ A $\beta_{40}$ fibril
				$^{13}\text{C}$	1.5	88			ILE $^{13}\text{C}$ , $^{15}\text{N}$ A $\beta_{40}$ fibril: Anle138b = 1:1.2 (Post-treatment condition)
2D $^{13}\text{C}$ - $^{13}\text{C}$ -DARR (20ms)	850, NEO	17 (3.2mm)	$^1\text{H}$ - $^{13}\text{C}$ -CP	$^1\text{H}$		80	100-80%	265K	ILE $^{13}\text{C}$ , $^{15}\text{N}$ A $\beta_{40}$ fibril: Anle138b = 1:1.2 (Pre-treatment condition)
				$^{13}\text{C}$	1.2	88			LYS $^{13}\text{C}$ , $^{15}\text{N}$ A $\beta_{40}$ fibril: Anle138b = 1:1.2 (Post -fibril condition)
2D $^{13}\text{C}$ - $^{13}\text{C}$ -RFDR (2.6ms)	600, Advance III e = 6 ~8 TEMTRIPol-1	10 (3.2mm)	$^1\text{H}$ - $^{13}\text{C}$ -CP	$^1\text{H}$		98	90-100%	100K (DNP)	LYS $^{13}\text{C}$ , $^{15}\text{N}$ A $\beta_{40}$ fibril: Anle138b = 1:1.2 (Pre-treatment condition)
				$^{13}\text{C}$	0.9	77			ILE $^{13}\text{C}$ , $^{15}\text{N}$ A $\beta_{40}$ fibril: Anle138b = 1:1.2 (Post-treatment condition)
2D $^{13}\text{C}$ - $^{13}\text{C}$ -DARR (50ms)	600, Advance III e = 6 ~8 TEMTRIPol-1	10 (3.2mm)	$^1\text{H}$ - $^{13}\text{C}$ -CP	$^1\text{H}$		70.8	90-100%	100K (DNP)	LYS $^{13}\text{C}$ , $^{15}\text{N}$ A $\beta_{40}$ fibril: Anle138b = 1:1.2 (Post-treatment condition)

				$^{13}\text{C}$	0.6				LYS $^{13}\text{C}$ , $^{15}\text{N}$ A $\beta_{40}$ fibril: Anle138b = 1:1.2 (Pre-treatment condition)
2D NHHc	600, Advance III e = 6 ~8 TEMTRIPol-1	10 (3.2mm)	$^1\text{H}$ - $^{15}\text{N}$ -CP	$^1\text{H}$	0.35	49	90-100%	100K (DNP)	$^1\text{H}$ , $^{13}\text{C}$ , $^{15}\text{N}$ A $\beta_{40}$ fibril: Anle138b = 1:1.2 (Pre-treatment condition)
				$^{15}\text{N}$		32			
			$^{15}\text{N}$ - $^1\text{H}$ --CP	$^{15}\text{N}$		32			$^1\text{H}$ , $^{13}\text{C}$ , $^{15}\text{N}$ A $\beta_{40}$ fibril: Anle138b = 1:1.2 (Pre-treatment condition)
				$^1\text{H}$	0.35	49	80-100%		
			$^1\text{H}$ - $^{13}\text{C}$ -CP	$^1\text{H}$		61	80-100%		
				$^{13}\text{C}$	0.6	84			
2D NHHc	600, Advance III e = 6 ~8 TEMTRIPol-1	10 (3.2mm)	$^1\text{H}$ - $^{15}\text{N}$ -CP	$^1\text{H}$	0.36	39	90-100%	100K (DNP)	LYS $^{13}\text{C}$ , $^{15}\text{N}$ A $\beta_{40}$ fibril: Anle138b = 1:1.2 (Post-treatment condition)
				$^{15}\text{N}$		31			
			$^{15}\text{N}$ - $^1\text{H}$ --CP	$^{15}\text{N}$		31			LYS $^{13}\text{C}$ , $^{15}\text{N}$ A $\beta_{40}$ fibril: Anle138b = 1:1.2 (Pre-treatment condition)
				$^1\text{H}$	0.6	39	80-100%		
			$^1\text{H}$ - $^{13}\text{C}$ -CP	$^1\text{H}$		67	80-100%		
				$^{13}\text{C}$	0.7	61			
2D NHHc	600, Advance III e = 6 ~8 TEMTRIPol-1	10 (3.2mm)	$^1\text{H}$ - $^{15}\text{N}$ -CP	$^1\text{H}$	0.5	43	90-100%	100K (DNP)	ILE $^{13}\text{C}$ , $^{15}\text{N}$ A $\beta_{40}$ fibril: Anle138b = 1:1.2 (Post-treatment condition)
				$^{15}\text{N}$		33			
			$^{15}\text{N}$ - $^1\text{H}$ --CP	$^{15}\text{N}$		33			ILE $^{13}\text{C}$ , $^{15}\text{N}$ A $\beta_{40}$ fibril: Anle138b = 1:1.2 (Pre-treatment fibril condition)
				$^1\text{H}$	0.3	43	80-100%		
			$^1\text{H}$ - $^{13}\text{C}$ -CP	$^1\text{H}$		98	80-100%		
				$^{13}\text{C}$	0.7	77			

**Supplementary Table 2 | Thermodynamic parameters obtained from ITC titrations of anle138b (in DLPG vesicle) or DLPG vesicle alone into L1 A $\beta$ <sub>40</sub> fibrils.**

Control titration results using DLPG vesicles without anle138b are shown in Supplementary Fig. 14 b, while titrations with DLPG vesicles containing anle138b are shown in Fig. 4 b and Supplementary Fig. 14a.

	[Anle138b (DLPG vesicle)] / [L1 A $\beta$ <sub>40</sub> fibril]	[DLPG vesicle] / [L1 A $\beta$ <sub>40</sub> fibril]
[Cell] ( $\mu$ M)	10.00	10.00
[Syringe] ( $\mu$ M)	100.00	100.00
N (sites)	0.72 $\pm$ 0.01	
KD ( $\mu$ M)	0.64 $\pm$ 0.068	
$\Delta$ H (kcal/mol)	-1.84 $\pm$ 0.039	
$\Delta$ G (kcal/mol)	-8.45	
-T $\Delta$ S (kcal/mol)	-6.62	

**Supplementary Table 3 | Cryo-EM structure determination statistics.**

	Post-treatment A $\beta$ <sub>40</sub> fibril	Pre-treatment A $\beta$ <sub>40</sub> fibril
<b>Data collection</b>		
Microscope	Titan Krios G2	Titan Krios G2
Voltage [keV]	300	300
Detector	K3	K3
Magnification	81,000	81,000
Pixel size [Å]	1.05	1.05
Defocus range [μm]	-0.7 to -2.4	-0.7 to -2.4
Exposure time [s/frame]	3.0	2.95
Number of frames	40	40
Total dose [e <sup>-</sup> /Å <sup>2</sup> ]	~40 (~1.0 e <sup>-</sup> /Å <sup>2</sup> /frame)	~40 (~1.0 e <sup>-</sup> /Å <sup>2</sup> /frame)
<b>Reconstruction</b>		
Micrographs	7,311	21,576
Box width [pixels]	250	250
Inter-box distance [pixels]	13	13
Picked segments (no.)	3,193,361	9,147,664
<b>Final map<sup>a</sup></b>		
Final segments [no.]	326,836	888,252
Final resolution [Å] (FSC=0.143)	2.79	2.76
Applied map sharpening B-factor [Å <sup>2</sup> ]	-114	-121
Symmetry imposed	C1	C1
Helical rise [Å]	2.35	2.35
Helical twist [°]	179.65	179.65

<sup>a</sup> Sharpened map and refined atomic model are provided as SI files.

**Supplementary Table 4 | Model building statistics.**

<b>Lipid-induced PM</b>	<b>Post-treatment A<math>\beta</math><sub>40</sub> fibril</b>	<b>Pre-treatment A<math>\beta</math><sub>40</sub> fibril</b>
<b>Initial model [PDB code]</b>	8ovk	8ovk
<b>Model composition<sup>a</sup></b>		
Chains	10	10
Non-hydrogen atoms	3060	3060
Protein residues	400	400
<b>RMS deviations</b>		
Bond lengths [Å ]	0.02	0.01
Bond angles [°]	2.23	2.09
<b>Validation</b>		
MolProbity score	1.68	1.70
Clashscore	5.86	6.19
<b>Ramachandran plot</b>		
Outliers [%]	0	0
Allowed [%]	5.26	5.26
Favored [%]	94.74	94.74

<sup>a</sup> Sharpened map and refined atomic model I.